$GlnA3_{Mt}$ is able to glutamylate spermine but it is not essential for the detoxification of spermine in *Mycobacterium tuberculosis*

Sergii Krysenko[1,2,12], Carine Sao Emani[3], Moritz Bäuerle[1], Maria Oswald[1], Andreas Kulik[1,2], Christian Meyners[4], Doris Hillemann[5], Matthias Merker[6], Inken Wohlers[7], Felix Hausch[4,11], Heike Brötz-Oesterhelt[2,8,10], Agnieszka Mitulski[1,8], Norbert Reiling[3,9,*], Wolfgang Wohlleben[1,2,10*]

[1] Interfaculty Institute of Microbiology and Infection Medicine Tübingen (IMIT), Department of Microbiology and Biotechnology, Auf der Morgenstelle 28, University of Tübingen, Tübingen, Germany

[2] Cluster of Excellence 'Controlling Microbes to Fight Infections', University of Tübingen, Auf der Morgenstelle 28, 72076 Tübingen, Germany

[3] Microbial Interface Biology, Research Center Borstel, Leibniz Lung Center, Parkallee 1-40, 23845 Borstel, Germany

[4] Institute of Organic Chemistry and Biochemistry, Technical University Darmstadt, Darmstadt, Germany

[5] National Reference Center for Mycobacteria, Research Center Borstel, Leibniz Lung Center, Parkallee 1-40, 23845 Borstel, Germany

[6] Evolution of the Resistome, Research Center Borstel, Leibniz Lung Center, Parkallee 1-40, 23845 Borstel, Germany

[7] Data Science, Research Center Borstel, Leibniz Lung Center, Parkallee 1-40, 23845 Borstel, Germany

[8] Interfaculty Institute of Microbiology and Infection Medicine Tübingen (IMIT), Department of Microbial Bioactive Compounds, Auf der Morgenstelle 28, University of Tübingen, Tübingen, Germany

[9] German Center for Infection Research (DZIF), Partner Site Hamburg-Lübeck-Borstel-Riems, Borstel, Germany

[10] German Center for Infection Research (DZIF), Partner Site Tübingen, Tübingen, Germany

[11] Centre for Synthetic Biology, Technical University of Darmstadt, 64283 Darmstadt, Germany

[12] Present address: Valent BioSciences, 1910 Innovation Wy Suite 100, Libertyville, IL 60048, USA

*equal contribution

Corresponding Author: Wolfgang Wohlleben, Department of Microbiology and Biotechnology, Interfaculty Institute of Microbiology and Infection Medicine Tübingen (IMIT), University of Tübingen, Auf der Morgenstelle 28, 72076 Tübingen, Germany. Tel.: +49 07071 29-76944, Fax: (07071) 29-5979, Email: wolfgang.wohlleben@biotech.uni-tuebingen.de.

Corresponding Author: Norbert Reiling, Microbial Interface Biology, Research Center Borstel, Leibniz Lung Center, Parkallee 1-40, 23845 Borstel, Germany. Tel.: +49 4537 188-4860, Email: nreiling@fz-borstel.de

Keywords: GS-like enzyme, GlnA3, glutamylation, polyamine metabolism, tuberculosis, infection, Rv3065

ABSTRACT

Mycobacterium tuberculosis is well adapted to survive and persist in the infected host, escaping the host immune response. Since polyamines, which are synthesized by infected macrophages are able to inhibit the growth of *M. tuberculosis*, the pathogen needs strategies to cope with toxic spermine. The actinomycete *Streptomyces coelicolor*, closely related to *M. tuberculosis* makes use of a gamma-glutamylation pathway to functionally neutralize spermine. We therefore considered whether a similar pathway would be functional in *M. tuberculosis*. In the current study we demonstrated that *M. tuberculosis* growth was inhibited by the polyamine spermine. Using a glutamine synthetase-based *in vitro* enzymatic activity assay we determined that $GlnA3_{Mt}$ (Rv1878) is a gamma-glutamylspermine synthetase. In an *in vitro* phosphate release assay we showed that purified His-Strep-$GlnA3_{Mt}$ as well as native $GlnA3_{Mt}$ prefer spermine as a substrate to putrescine, cadaverine, spermidine or other monoamines and amino acids, suggesting that $GlnA3_{Mt}$ may play a specific role in the detoxification of the polyamine spermine. However, the deletion of the *glnA3* gene in *M. tuberculosis* did not result in growth inhibition or enhanced sensitivity of *M. tuberculosis* in the presence of high spermine concentrations. Subsequent RNAsequencing of *M. tuberculosis* bacteria revealed that the gene cluster consisting of the efflux pump-encoding *rv3065-rv3066-rv3067* genes is upregulated upon spermine treatment, suggesting its involvement in bacterial survival under elevated spermine concentrations.

IMPORTANCE

Antibiotics for the treatment of *Mycobacterium tuberculosis* infections attack classical bacterial targets, such as the cell envelope or the ribosome. Upon *M. tuberculosis* infection macrophages synthesize the polyamine spermine which - at elevated concentrations - is toxic for *M. tuberculosis*. Based on our investigations of spermine resistance in the closely related actinomycete *Streptomyces coelicolor*, we hypothesized that the glutamyl-sperminesynthetase GlnA3 may be responsible for resistance against toxic spermine. Here we show that the mycobacterial glutamyl-sperminesynthetase indeed can inactivate spermine by glutamylation. However, GlnA3 is probably not the only resistance mechanism since a *glnA3* mutant of *M. tuberculosis* can survive under

spermine stress. Gene expression studies suggest that an efflux pump may participate in resistance. The functional role of $GlnA3_{Mt}$ as well as of the spermine transporter in the pathogenicity of *M. tuberculosis* is of special interest for their validation as new targets of novel anti-tubercular drugs.

1. INTRODUCTION

Worldwide, tuberculosis (TB) remains the most prevalent, persisting and difficult to treat infectious disease and is associated with high mortality. In 2021, an estimated 10.6 million people developed TB disease, with an estimated 1.6 million deaths (1). Tuberculosis is caused by pathogenic mycobacteria of the *Mycobacterium tuberculosis* complex (MTBC), which are well adapted to survive and persist within infected patients (2). An overall increase in the global burden of multidrug-resistant (MDR) and rifampicin-resistant (RR) TB severely jeopardizes control of the TB epidemic as envisaged by the WHO End TB strategy. MDR/RR-TB has been identified on all continents with approximately 450.000 cases reported in 2021 (1). Treatment of MDR-TB infections is of particular difficulty due to the extended duration, poor safety, and high costs associated. Several antibiotics are effective in treating MDR-TB infections; however, these drugs often show limited efficacy and their use is coupled with diverse side-effects. Thus, the identification of pathways that are essential for mycobacterial growth *in vivo* would provide new targets for the rational design of more effective anti-TB agents that could be active against MDR-TB.

Polyamines are small aliphatic polyvalent cations, predominantly derived from amino acids such as ornithine, arginine, and lysine (3). They are widely distributed in nature and are present in all organisms, with the most common cellular polyamines being putrescine, cadaverine, spermidine and spermine. Polyamines have been implicated in a wide range of biological processes, and their intracellular levels are elevated predominantly during exposure to various stress conditions (3, 4). Thus, intracellular polyamine concentrations are tightly regulated by cellular metabolic pathways (4), as polyamine excess has been proven toxic for prokaryotic and eukaryotic organisms and can lead to cell death (5-8). Polyamines are able to interact with negatively charged molecules like RNA, DNA, proteins, polyphosphate, and phospholipids (9). Consequently, an imbalance in polyamine metabolism can significantly affect cellular homeostasis. An excess of polyamines can be detoxified by modifications such as glutamylation. Detoxification is also the first step in subsequent polyamine assimilation as C/N sources under nutrient limiting conditions. Polyamine catabolism was investigated in several bacterial species revealing that the polyamine utilization pathway is not universal for all bacteria. This process was studied extensively in Gram-negative

bacteria such as *E. coli* and *P. aeruginosa* POA1. Polyamine utilization was reported to occur via the aminotransferase pathway (10), the γ-glutamylation pathway (10-12), the direct oxidation pathway for putrescine, and the spermine/spermidine dehydrogenase pathway. *E. coli* and *B. subtilis* were shown to acetylate spermidine (12-15), whereas in the actinobacterial model organism *Streptomyces coelicolor*, the γ-glutamylation pathway was demonstrated (16-18).

S. coelicolor was shown to synthesize two functional, glutamine synthetase-like (GS-like) enzymes for polyamine glutamylation: the gamma-glutamylpolyamine synthetases $GlnA2_{Sc}$ and $GlnA3_{Sc}$. $GlnA3_{Sc}$ was reported to be a central enzyme for the γ-glutamylation pathway in *S. coelicolor*, and is highly specific for spermine (16, 17). In *S. coelicolor*, $GlnA3_{Sc}$ permits detoxification and subsequent utilization of polyamines as a nitrogen source and is indispensable for bacterial survival under high polyamine concentrations (16). Recent *in silico* analysis of *glnA*-like genes across the actinobacterial phyllum revealed numerous orthologues (*glnA2*, *glnA3* and *glnA4*) that code for proteins potentially involved in the colonization, persistence and survival of bacteria across diverse habitats (18).

Little is known about polyamine utilisation and its regulation in *M. tuberculosis.* In *M. tuberculosis*, $GlnA3_{Mt}$ has been annotated and classified as “GS-like” (19, 20). While the function, regulation and involvement of the glutamine synthetase (GS_{Mt}) (GlnA1, Rv2220) in mycobacterial pathogenesis were extensively studied (19), the function of $GlnA3_{Mt}$ (Rv1878) so far remains unclear. Because many steps of nitrogen metabolism in *S. coelicolor* are nearly identical to those of *M. tuberculosis* (21-23), we hypothesized that *M. tuberculosis* might also exert a similar capacity for polyamine detoxification. The current study is the first to investigate polyamine metabolism in *M. tuberculosis* and the role of $GlnA3_{Mt}$ in this process.

2. RESULTS

$GlnA3_{Mt}$ from *M. tuberculosis* restores the growth of the polyamine-deficient *S. coelicolor glnA3* mutant in polyamine-containing medium

As reported previously, $GlnA3_{Sc}$ confers the ability of *S. coelicolor* M145 to utilize polyamines as a sole nitrogen source (16). In order to test for a similar predicted

function of the GlnA3$_{Mt}$ enzyme, the *glnA3*$_{Mt}$ gene was used for heterologous complementation of the *S. coelicolor* M145 Δ*glnA3*$_{Sc}$ mutant. The integrative vector pRM4 carrying a single copy of the *glnA3*$_{Mt}$ gene was integrated into the genome of the *S. coelicolor* M145 Δ*glnA3*$_{Sc}$ mutant. Successful integration of the construct in the *S. coelicolor* M145 genome was confirmed by PCR and sequencing. The phenotype of the complemented Δ*glnA3*$_{Sc}$ mutant was analyzed on complex, nitrogen-replete media (LB-agar, R5-agar), as well as on defined Evans-agar supplemented with single nitrogen sources (ammonium, L-glutamine or the polyamines putrescine, spermidine, spermine). Growth and morphology of the parental *S. coelicolor* M145 strain, the Δ*glnA3*$_{Sc}$ mutant and the Δ*glnA3*$_{Sc}$ complemented with *glnA3*$_{Sc}$ or *glnA3*$_{Mt}$ were monitored on solid media in a time range between 3 and 12 days of incubation at 30˚C. The strains grew well on complex media (LB and R5) and on the defined Evans medium supplemented with ammonium and glutamine (Tab. 1).

Tab. 1. Physiological role of the *glnA3*$_{Mt}$ gene product in the *S. coelicolor glnA3* mutant grown in the presence of polyamines and other nitrogen sources.

Medium	**M145 (WT)**	**Δ*glnA3*$_{Sc}$**	**Δ*glnA3*$_{Sc}$ +*glnA3*$_{Mt}$**	**Δ*glnA3*$_{Sc}$ +*glnA3*$_{Sc}$**
LB-Agar	+++	+++	+++	+++
R5-Agar	+++	+++	+++	+++
Evans-Agar + NH_4Cl (50 mM)	+++	+++	+++	+++
Evans-Medium + Glutamine (50 mM)	+++	+++	+++	+++
Evans-Medium + Putrescine (200 mM)	+++	-	+	++
Evans-Medium + Spermidine (25 mM)	+++	-	+	++
Evans-Medium + Spermine (25 mM)	+++	-	+	++

Note: +: poor growth, ++: moderate growth, +++: strong growth; -: no growth.

The Δ*glnA3*$_{Sc}$ mutant was not able to grow on the defined Evans medium with polyamines as the only nitrogen source as previously reported (16). The heterologous complementation of the Δ*glnA3*$_{Sc}$ mutant by the *glnA3*$_{Mt}$ gene partially restored its growth on defined Evans medium supplemented with either putrescine, spermidine or spermine as the only nitrogen source (Tab. 1, Suppl. Fig. 1) thus demonstrating the functional equivalence of GlnA3$_{Sc}$ and GlnA3$_{Mt}$. Interestingly, GlnA3$_{Mt}$ rescued growth of the *S. coelicolor* Δ*glnA3*$_{Sc}$ mutant grown on putrescine, although this enzyme has low substrate specificity towards short-chain polyamines (see Fig. 2). This indicates that the native GlnA2 enzyme, which is highly specific towards putrescine (16, 17), in the *S. coelicolor* test system could compensate for the lack of specificity towards putrescine by GlnA3$_{Mt}$, allowing to rescue the growth of the mutant.

GlnA3$_{Mt}$ catalyzes gamma-glutamylation of spermine and spermidine *in vitro*, but not of putrescine or cadaverine

To elucidate the biochemical function of GlnA3$_{Mt}$ and to confirm that GlnA3$_{Mt}$ is able to catalyze the predicted glutamylation reaction of organic polyamines, we applied a previously validated HPLC/mass spectrometry (HPLC/MS)-based assay (17). For this purpose, recombinant *glnA3*$_{Mt}$ was purified from *Escherichia coli* BL21 as a His- and Strep-tag fusion protein, with subsequent removal of the affinity tags. Analysis of the final product by size-exclusion chromatography supported the predicted dodecameric quaternary structure of GlnA3$_{Mt}$ (Fig. 1). The catalytic activity of purified GlnA3$_{Mt}$ was then tested by incubation with various polyamines in relevant reaction mixtures and the products analyzed using HPLC/MS analysis in negative MS mode (Fig. 1, reaction educts and products and their respective masses are depicted in Suppl. Fig. 2). Our data show that GlnA3$_{Mt}$ accepted glutamate and spermine as substrates in an ATP-dependent manner, resulting in the expected *m/z* for glutamylspermine. No glutamylated putrescine, cadaverine and spermidine were detected. The GlnA3$_{Mt}$-catalyzed reaction generated a product with the mass-to-charge ratio of *m/z* 331, corresponding to the calculated mass of the gamma-glutamylspermine, supporting the hypothesis that GlnA3$_{Mt}$ functions as a gamma-glutamylspermine synthetase (Fig. 1).

199

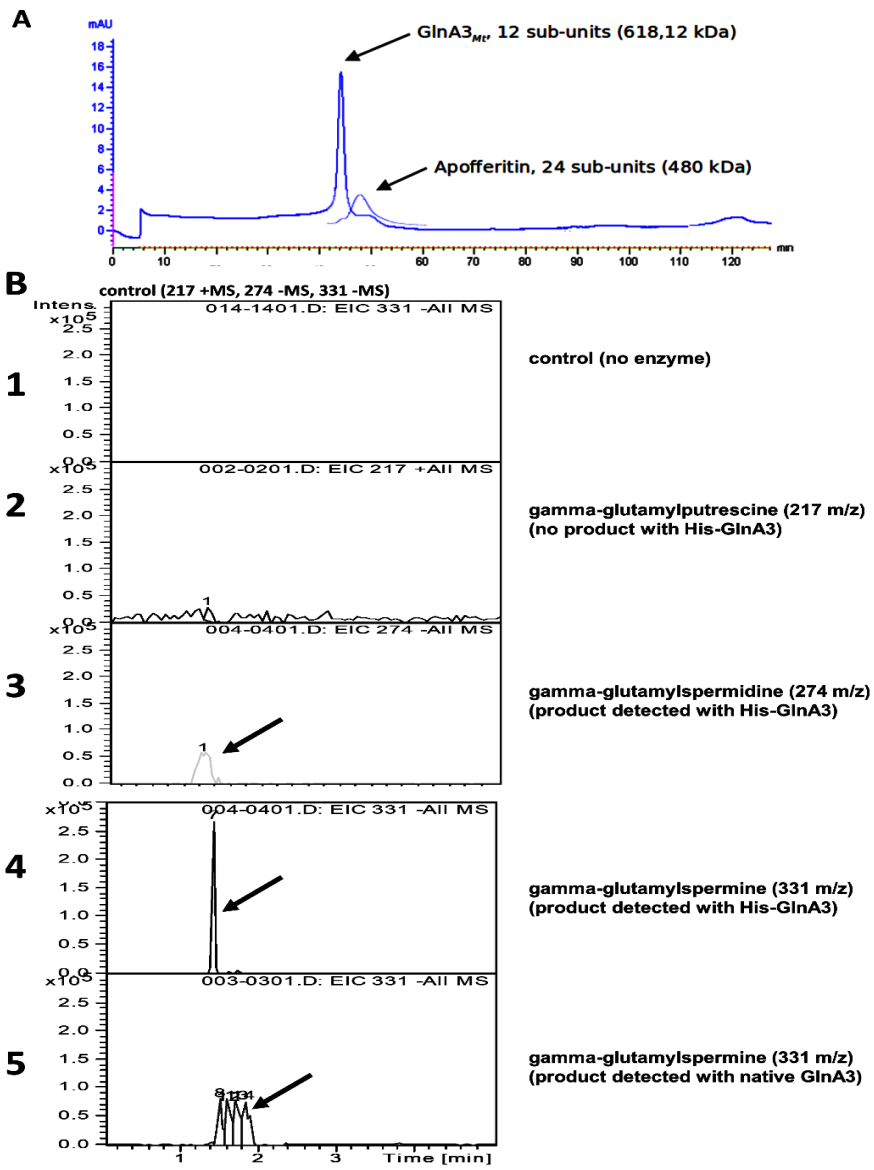

Fig. 1. Purification of GlnA3Mt and generation of glutamylated spermine and spermidine by GlnA3Mt in an in vitro assay proved by the HPLC/ESI-MS analysis. A) purification of GlnA3Mt by size-exclusion chromatography (SEC). SEC supported the putative dodecameric quaternary structure of the enzyme. Pre-ordered apoferritin protein was used as a control for molecular mass estimation (elution profile shown in part). B) mass spectra chromatograms for the control detecting glutamylated putrescine, spermidine and spermine in a sample without GlnA3Mt enzyme (1), gamma-glutamylputrescine (m/z 217) (2), gamma-glutamylspermidine (m/z 274) (3), gamma-glutamylspermine (m/z 331), GlnA3Mt purified by SEC with the Tag (4), gamma-glutamylspermine (m/z 331), His-Strep-GlnA3Mt purified by affinity chromatography without the Tag (5). Glutamylated spermine and spermidine could be detected.

200

201

202 **Spermine is a preferred substrate for His-Strep-GlnA3$_{Mt}$**

203 To study the substrate specificity of GlnA3$_{Mt}$ and its kinetic parameters, an adapted GS

204 activity assay (24) based on the detection of inorganic phosphate (Pi) (released from

ATP hydrolysis) was employed. Recombinant His-Strep-GlnA3$_{Mt}$ or the *S. coelicolor* orthologue were incubated with test substrates (polyamines, monoamines, ammonium and amino acids) and required cofactors for 5 minutes, followed by quantification of inorganic phosphate release. All substrates were tested at 50 mM concentration as determined in a previous study in the *S. coelicolor* model system (16, 17). The results revealed that GlnA3$_{Mt}$ can accept polyamines and amino acids like methionine as substrates, but overall, it is very specific for spermine.

In order to compare the substrate specificity of GlnA3$_{Mt}$ with its homologue GlnA3$_{Sc}$, which was characterized as a gamma-glutamylpolyamine synthetase in *S. coelicolor*, the adapted GS activity assay was applied as described above (Fig. 2).

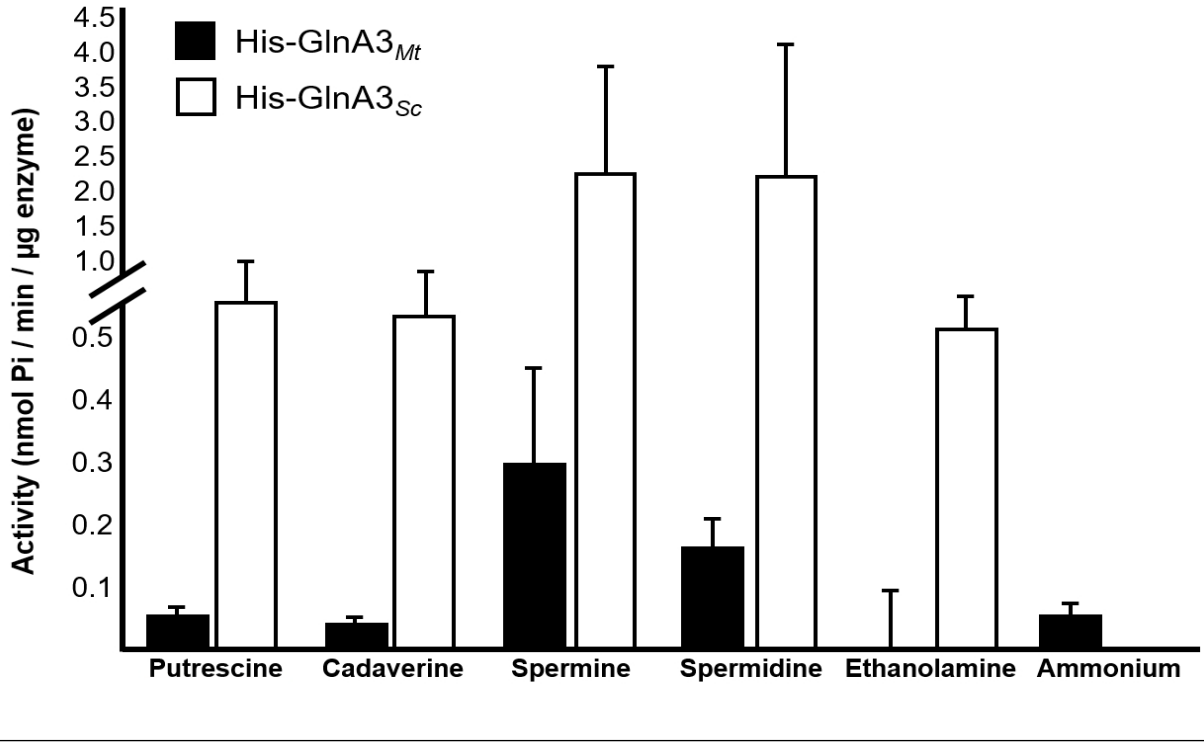

Fig. 2. Specific activity of His-GlnA3$_{Mt}$ and His-GlnA3$_{Sc}$ with different nitrogen containing substrates. All substrates were at 50 mM. The mean value of n=3 biological replicates with n=3 technical replicates each with standard error is shown.

The analysis revealed that His-Strep-GlnA3$_{Mt}$ prefers spermine and spermidine as substrates. This finding is in contrast to His-GlnA3$_{Sc}$ which accepts also other polyamines (Fig. 2) and possesses a higher specific activity for all tested substrates except ammonium. This result demonstrated a rather specific spermine activity of

GlnA3$_{Mt}$ from *M. tuberculosis*, which was not observed for its homolog GlnA3$_{Sc}$ from *S. coelicolor*.

In order to exclude putative effects of the tags on the obtained results, we independently assessed the activity of native GlnA3$_{Mt}$ with regard to the usage of putrescine, cadaverine, spermidine and spermine. The enzyme was purified as a fusion protein with the SUMO-Tag, which was subsequently removed by cleavage. The enzymatic activity of the native GlnA3$_{Mt}$ version was tested and compared with the His-Strep-GlnA3$_{Mt}$. Although the native GlnA3$_{Mt}$ revealed overall higher enzymatic activity than the tagged version in *in vitro* assays, both GlnA3$_{Mt}$ variants showed significantly higher activity with spermine compared to other polyamine substrates (Suppl. Fig. 3). The effect remained the same after 1h of additional incubation.

GlnA3$_{Mt}$, a predicted gamma-glutamylpolyamine synthetase structurally resembles GlnA3$_{Sc}$

GlnA3$_{Mt}$ shares 52% amino acid similarity across the full length sequence to GlnA3$_{Sc}$ from *S. coelicolor* M145 suggesting that the two orthologues may also share a similar tertiary structure (16).

In order to study the structural properties of GlnA3$_{Mt}$ in the absence of experimental data, a homology modelling approach was used. The cloud-based software SWISS-MODEL (25) was used to generate an *in silico* 3D model of the protein, based on the available amino acid sequence and a template model; in this case the previously solved structure of GlnA1$_{Mt}$ was used (26-30).

The GlnA3$_{Mt}$ model structure of *M. tuberculosis* comprises 12 identical subunits (Suppl. Fig. 4, A) organized in 2 rings, 6 sub-units in each (Suppl. Fig. 4, B), and one active site per sub-unit. Similar to both the solved GlnA$_{Mt}$ structure (27) and the GlnA3$_{Sc}$ model (16), a tunnel-like structure is observed in each active site of GlnA3$_{Mt}$ (Suppl. Fig. 4 B, C) comprising individual substrate binding sites for ATP, glutamate and ammonium. To improve confidence in the *in silico* data, we generated further models of GlnA3$_{Mt}$ using 20 different templates originating from various phyla of actinobacteria, proteobacteria, apicomplexa and cyanobacteria. Model quality was then assessed based on GMQE, QMEAN, and MolProbity scores (31), and Ramachandran analysis (Suppl. Fig. 4, D) (32, 33). Structure prediction was afterwards verified based on Alphafold predictions.

The Alphafold prediction of the monomers matched the homology model monomer generated by the Chimera software.

The high diversity of templates used allowed the identification of conserved areas between the $GlnA3_{Mt}$ structure and other bacterial homologues. Across all analyzed proteins it was observed that most of the conserved amino acid residues were located in the active site of each monomer, namely in the glutamate, metal ions and ATP binding sites. The active site of $GlnA3_{Mt}$ contains 9 out of 12 conserved amino acid residues at the ammonium binding site compared to the described gamma-glutamylpolyamine synthetase $GlnA3_{Sc}$, thought possessing more space on the loop for polyamine binding (no A169 residue in $GlnA3_{Mt}$) (Fig. 3, Tab. 2).

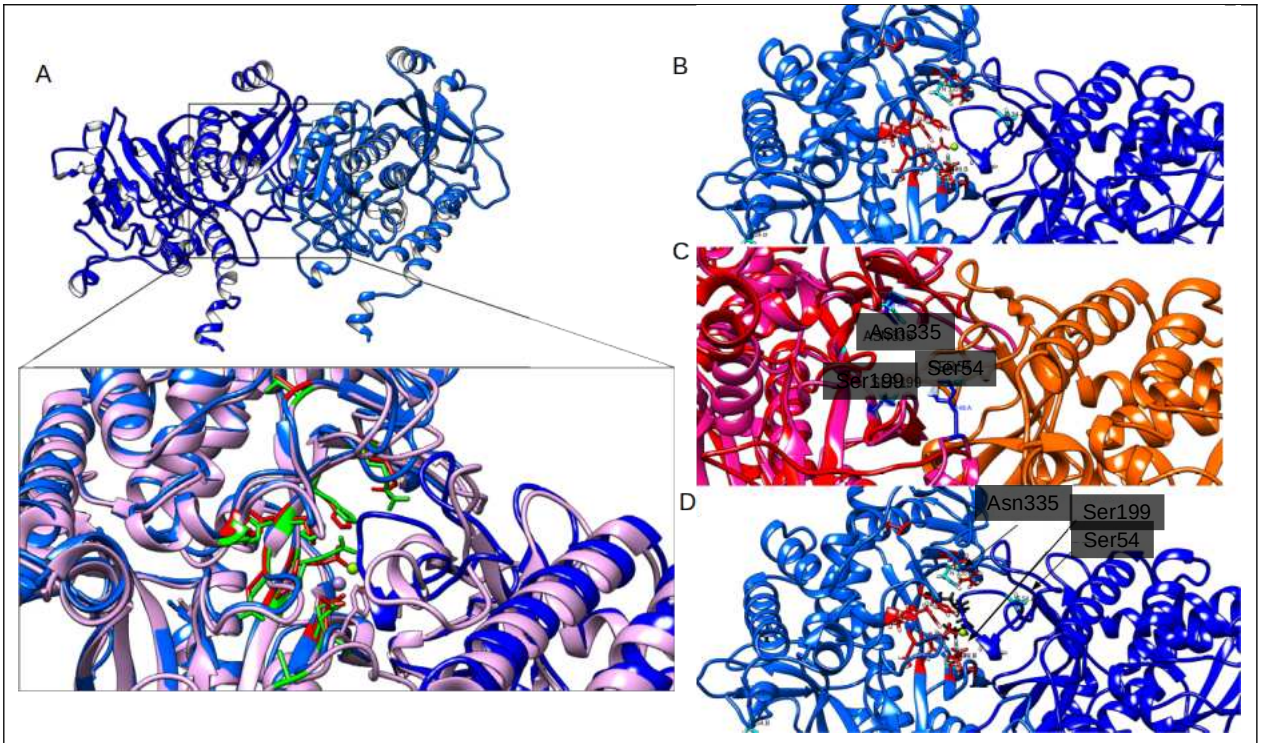

Fig. 3 A) Structural alignment of the 3D model structure of the $GlnA3_{Mt}$ enzyme. Based on and superposed with the $GlnA_{Mt}$ template (PDB code 1BVC (27). Superposition of the $GlnA3_{Sc}$ (violet) and $GlnA3_{Mt}$ (blue) models with depicted key amino acids identified in $GlnA3_{Sc}$ (green, from (16) and $GlnA3_{Mt}$ (red) (see Tab. 2). B) Constellation of amino acid residues crucial for polyamine substrate binding in $GlnA3_{Mt}$. The residues selected for site-directed mutagenesis i.e. Ser54, Ser199 and Asn335 (cyan) are depicted in the active site of $GlnA3_{Mt}$ among key residues in the binding pocket (red), C) computed localization of the spermine substrate (black) by molecular docking in the best scored dock position, D) structural alignment of structure models of two sub-units of $GlnA3_{Mt}$ (red and orange) overlaid with the crystal structure of $PauA7_{Pa}$ (violet).

Tab. 2

Superposition of residues in $GlnA3_{Sc}$ and $GlnA3_{Mt}$												
$GlnA3_{Sc}$	E151	E153	E207	E214	H263	N260	G261	R316	H265	R339	W327	A169
$GlnA3_{Mt}$	E137	E139	E190	E197	H246	S243	G244	R299	H248	R322	A310	none

Site-directed mutagenesis of $GlnA3_{Mt}$ defines structural features important for spermine binding

In order to study the role of distinct residues of $GlnA3_{Mt}$ in catalytic activity and substrate recognition, a site-directed mutagenesis approach was undertaken. This approach relied on molecular docking with spermine and structural/sequence alignments with the available crystal structure of the gamma-glutamyl(mono-)polyamine synthetase from *P. aeruginosa* $PauA7_{Pa}$ (34), which is a functional homolog of $GlnA3_{Mt}$. The comparison enabled the identification of potential key amino acids in the active site of $GlnA3_{Mt}$. For example, Ser54 is part of the loop closing the active site, which is essential for substrate stabilization (34). In addition, Ser199 is a part of the so-called Tyr loop which partly forms the tunnel-like structure of the active site. Ser199 may also be part of the catalytic triad in $GlnA3_{Mt,}$ however this is yet to be defined. Finally, Asn335 forms part of a second loop structure that closes the active site (Fig. 3, A, C). The molecular modeling revealed that spermine may form interactions with those identified amino acid residues (Fig. 3, B). Based on these observations, these three amino acids (Ser54, Ser199, Asn335) were mutated via site directed mutagenesis and the respective recombinant proteins purified. Constructs containing the $glnA3_{Mt}$* variants containing a mutation were produced as previously described for the WT enzyme. Conducting activity and substrate specificity testing via the GS-based *in vitro* assay, it was demonstrated that the $GlnA3_{Mt}$Ser199 enzyme variant exhibited no activity for any polyamine, in contrast to the WT and $GlnA3_{Mt}$Ser54 and $GlnA3_{Mt}$Asn335 variants (Fig. 4). These results were further verified by HPLC/MS analysis of reaction products (Suppl. Fig. 5).

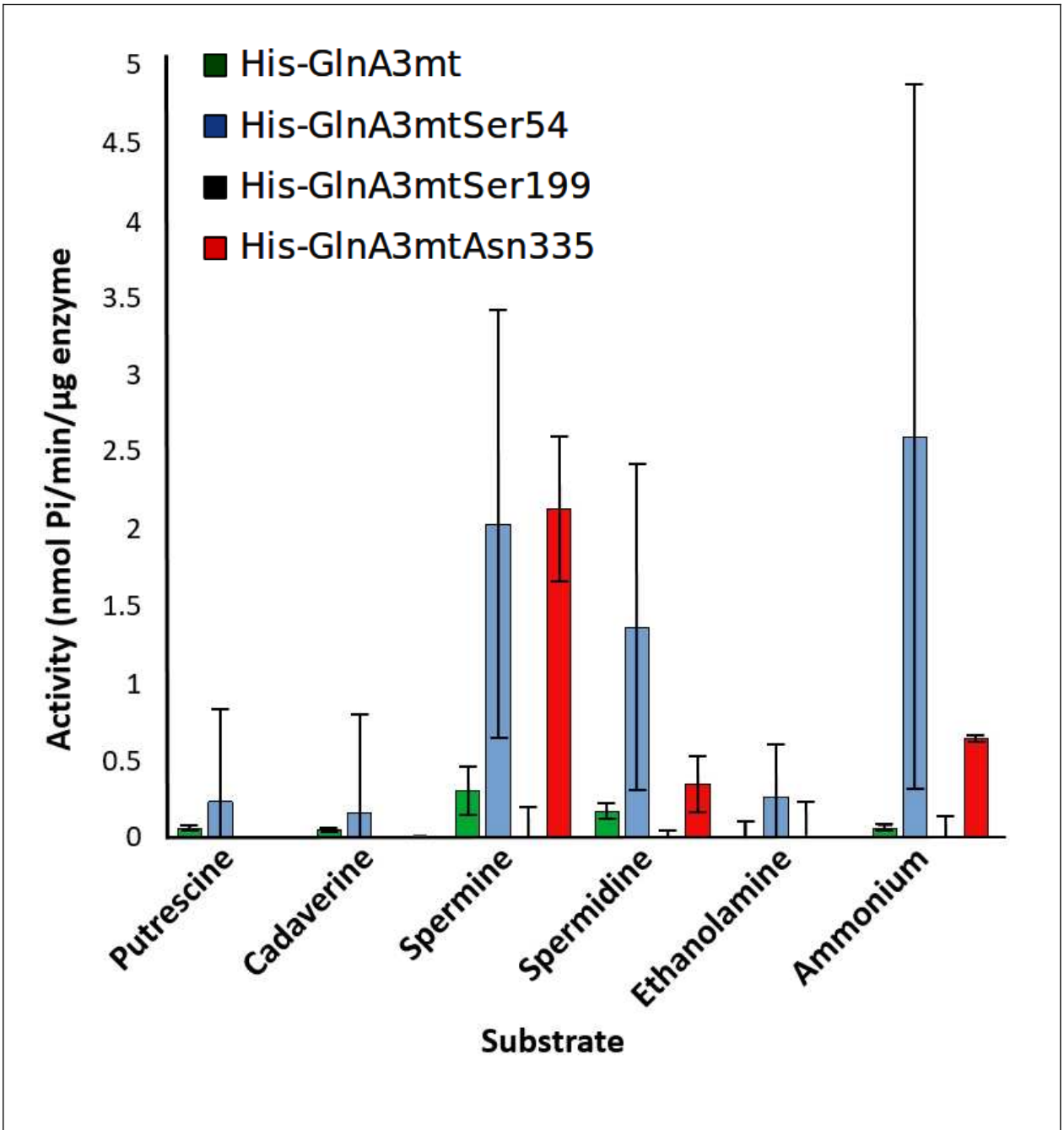

Fig. 4. Specific activity of His-Strep-GlnA3$_{Mt}$ and His-Strep-GlnA3$_{Mt}$* variants with different nitrogen-containing substrates. All substrates are at a concentration of 50 mM. The mean value of n=3 biological replicates with n=3 technical replicates each with standard error is shown.

M. tuberculosis is able to detoxify the polyamine spermine

In order to assess potential toxicity of spermine against *M. tuberculosis*, we first investigated its effect on *M. tuberculosis* in the standard *M. tuberculosis* laboratory culture medium, 7H9, supplemented with albumin, dextrose and sodium chloride (ADS).

Growth curve analyses revealed that 5 mM of spermine was required to achieve 90% inhibition (IC_{90}) of *M. tuberculosis* growth (Fig. 5, A) with 50% inhibition (IC_{50}) at 3 mM. Similar values were obtained irrespective of the supplement (ADS or OADC, see material and methods section) in a fluorescence-based test system employing an *M. tuberculosis* H37Rv strain expressing a red fluorescent protein (Suppl. Fig. 6, A and 6, B).

We then investigated the activity of spermine in a minimal medium without supplement (Sauton's media), and observed that spermine was able to inhibit the growth of *M. tuberculosis* but at a substantially lower concentration (IC_{90} of 180-320 µM, IC_{50} of 80 µM (Fig. 5, B). Whenever albumin was added to the minimal media (3 mg/ml), the activity of spermine was inhibited (Fig. 5, C-E). This in accordance with previous studies demonstrating that spermine conjugates with albumin (35) thereby likely explaining the high MIC (low activity) of spermine in 7H9 standard media, containing albumin in the supplement.

In an additional we attempted to detect the glutamylated spermine in *M. tuberculosis,* the MTB Beijing strain (WT variant) and in the naturally occurring *glnA3* Beijing mutant were analysed by LC/MS. Low amounts of gamma-glutamylspermine were detected in these strains (Suppl. Fig. 7).

Since the Δ*glnA3* mutant was not more sensitive to Spermine relative to the wild-type, we referred to previous studies showing the implication of $GlnA3_{MT}$ in nitrogen metabolism (19). Therefore, we investigated the ability of the mutant to use spermine as a sole C/N source. We found that the survival of the mutant was enhanced in the presence of spermine as the sole C/N source (Suppl. Fig. 8). This indicates that the mutant is able to metabolize spermine as a C/N source.

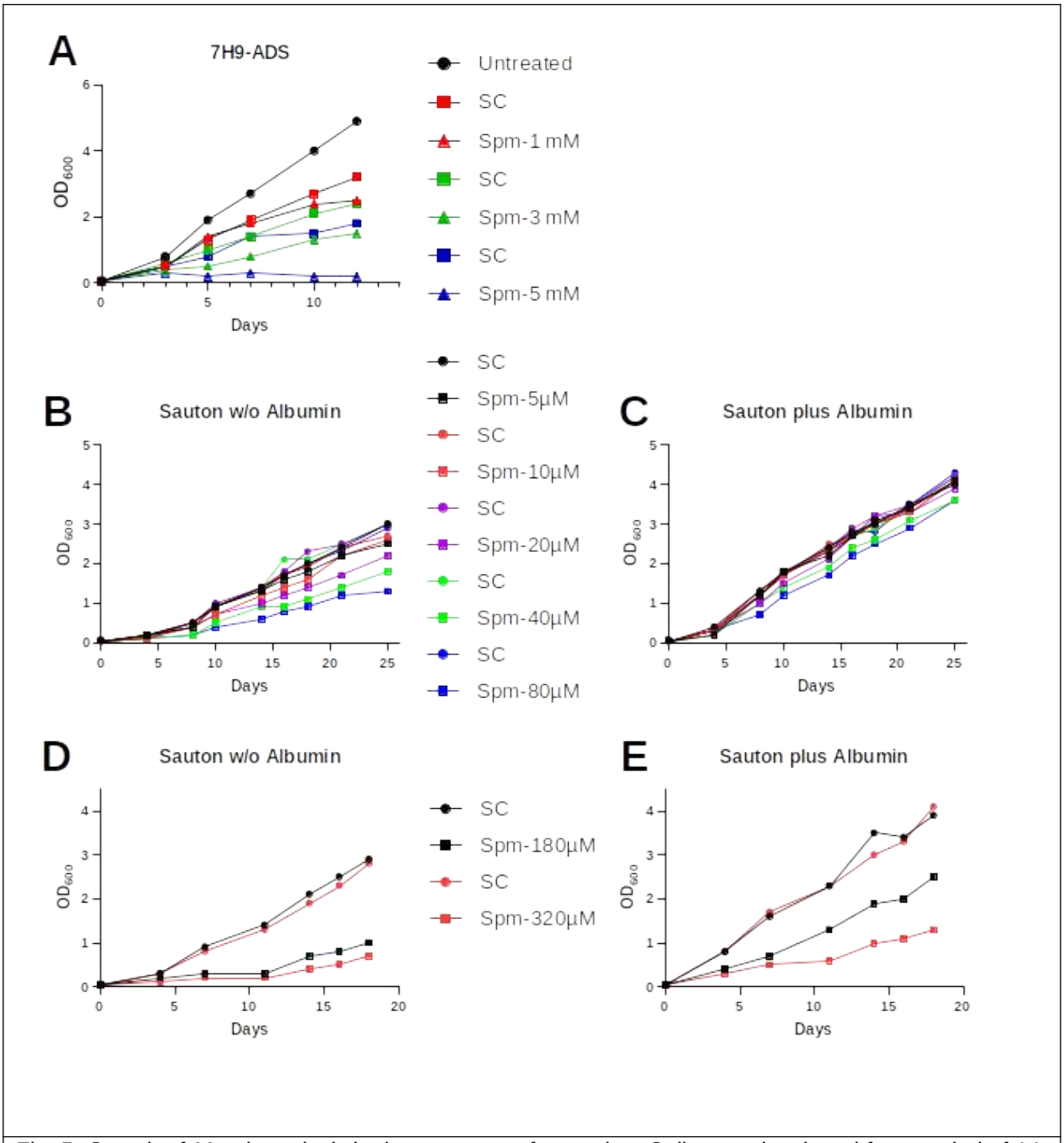

Fig. 5. Growth of *M. tuberculosis* in the presence of spermine. Cells were incubated for a period of 14-26 days in **(A)** 7H9 media supplemented with ADS in the presence of 0.5-5 mM spermine (shown is one representative experiment out of four), **(B-E)** Sauton media in the presence of 5-80 µM (B, C) or 180-320 µM spermine (D, E) either incubated without (w/o) albumin (B, D) or with added albumin (C, E). SC: solvent control (DMSO) ; Spm: spermine

The *M. tuberculosis ΔglnA3*$_{Mt}$ mutant is not sensitive to spermine

As $GlnA3_{Sc}$ plays a fundamental role in the survival of *S. coelicolor* at high spermine concentrations (16), we decided to employ a genetic approach to interrogate whether the same is true in *M. tuberculosis*. To this end, we constructed an unmarked, in-frame $glnA3_{Mt}$-deletion mutant of *M. tuberculosis*, as described in Materials and Methods (36, 37). The $\Delta glnA3_{Mt}$ (*Δrv1878*) mutant was identified by PCR, and validated by Southern blotting and targeted genome sequencing. The successful generation of the Δ*rv1878* mutant demonstrates that *rv1878* is not an essential gene in *M. tuberculosis* as previously indicated (38, 39).

The susceptibility of the mutant to spermine relative to the wild-type was first investigated by the broth microdilution method. The MIC was found to be similar to the wild-type's. Next, spermine sensitivity was investigated by monitoring the growth of the strains in the presence of sub-inhibitory concentrations of spermine (half the MIC), Again, no difference in growth rate was observed between the mutant and wild-type (Fig 6, C and 6, D). Finally, in order to eliminate the possibility that the difference between the mutant and the wild-type was too small to detect with standard growth curve analyses or by MIC determinations, we evaluated the effect of spermine treatment on bacteria by determining colony-forming units (CFU). Three hours of treatment at excess concentrations of spermine (2 mM) in Sauton's media revealed no difference in CFUs between the tested strains. In summary, all methods revealed that the mutant did not show an elevated sensitivity to spermine (Fig. 6, C, D, and E).

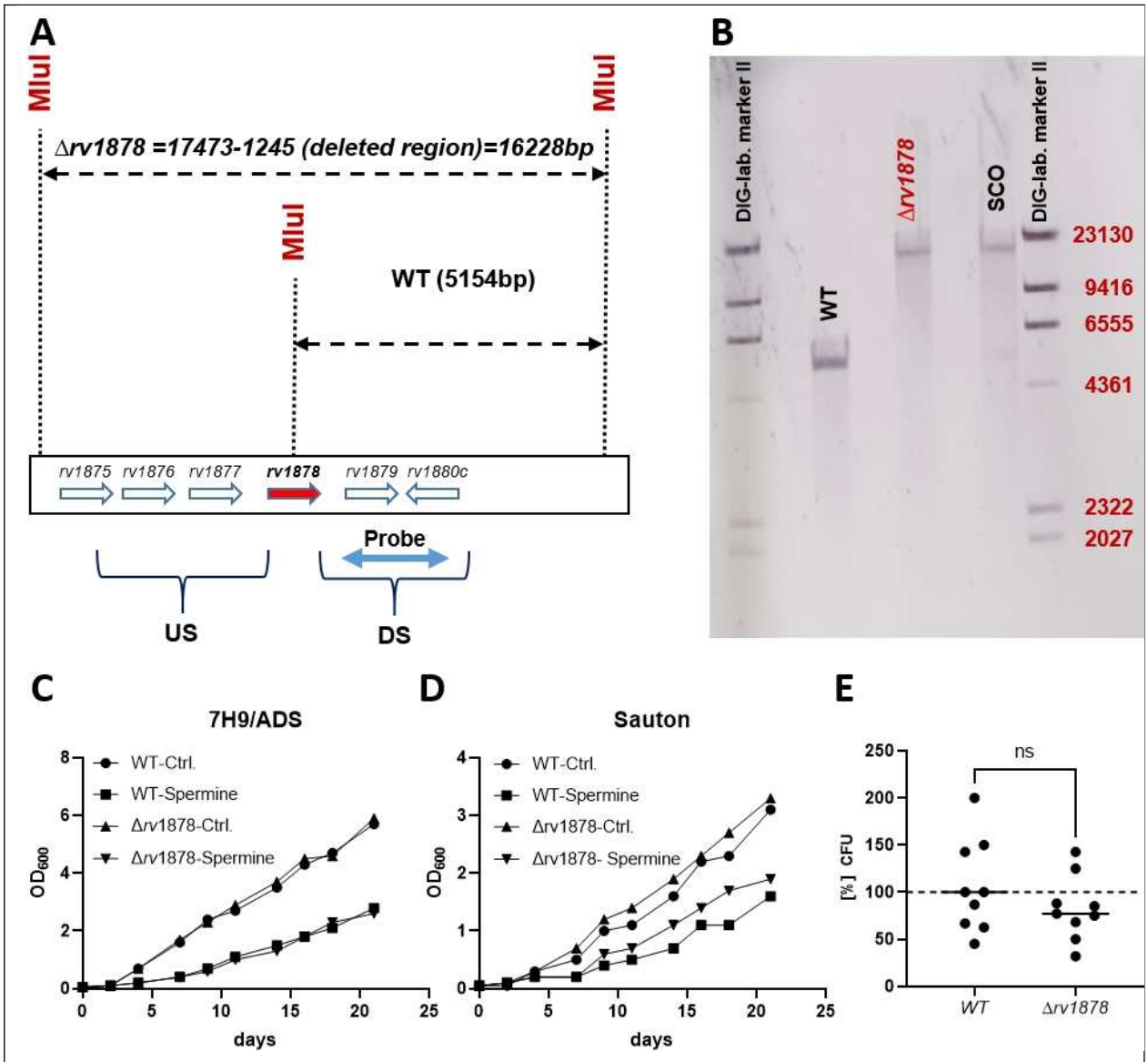

Fig. 6. Generation and characterization of the *M. tuberculosis* Δ*glnA3* mutant relative to the wild-type. A and B) Southern blotting analyses to confirm gene deletion. The construct was designed such that the wild type DNA would yield a smaller band (5,154 bp) when digested with the enzyme *Mlu*I and hybridized with the probe flanking the DS (downstream) region, while the mutant DNA would yield a bigger band (16,228 bp) since *Mlu*I would not be able to cut in *glnA3*, since the restriction site has been deleted. The single cross-over mutant has both the wild-type and mutant bands. C) Sensitivity of the mutant relative to the wild type to 3 mM (1/2 MIC) spermine determined by growth curve analyses in 7H9 media, D) Sensitivity of the mutant relative to the wild-type to 80 µM (1/2 MIC) spermine determined by growth curve analyses in Sauton's media, E) Sensitivity of the mutant relative to the wild type to 2 mM spermine determined by CFU counts and survival estimation (relative to the untreated control) in Sauton media for 3 hours). US, upstream; SCO Single cross over; ns, not significant)

342

343

RNAseq analysis: Spermine does not regulate *Rv1878* and the adjacent mycobacterial genes

To investigate if *rv1878 (glnA3$_{Mt}$)* and the adjacent genes (*rv1876*, *rv1877* and *rv1879*), were regulated by spermine stress, we initially performed RNAseq analysis of the wild-type bacteria cultured in 7H9 media and treated at half the MIC (3 mM), relative to the untreated control. A substantial change in gene expression of *rv1876*, *rv1878* and *rv1879* was not observed (less than 2fold (Fig. 7, A), validated by RT-PCR data (Fig. 7, B). Of note we observed in RNAseq analyses that *rv1877* displayed a 4-fold upregulation i.e. log2 median fold change of 1.7), which was shown to be even 10-fold enhanced, when validated by RT-PCR (Fig. 7, B) in 7H9 media conditions. Rv1877, a member of Major Facilitator Superfamily (MFS) has only recently been described as a multidrug efflux pump in *M. tuberculosis* (40). Since albumin could have possibly interfered with the activity of spermine (as discussed above) we repeated the experiment with medium lacking albumin to apply a more pronounced spermine stress. To this end RNA was sequenced from bacteria cultured in Sauton's media, yet the regulation of all four genes found in this cluster was not altered by spermine stress (Fig. 7, C). These data show that *rv1877* is apparently upregulated only in supplemented 7H9 Media but not in Sauton's media.

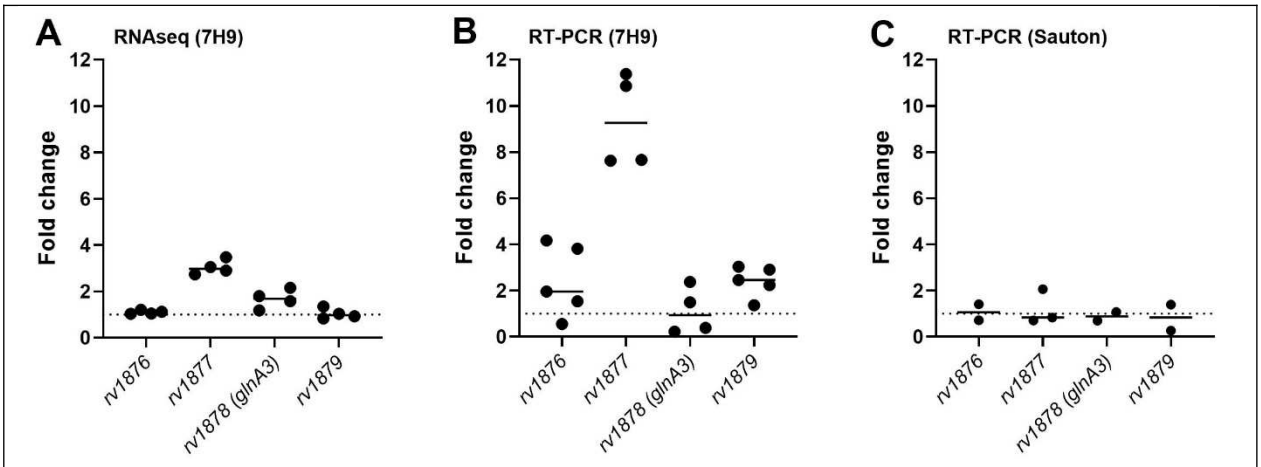

Fig. 7. Alteration of the expression level of selected genes in *M. tuberculosis* WT. The expression was determined by RNAseq (A) and RT-PCR analysis (B, C) in 7H9 (A, B) and Sauton´s (C) medium. Predicted gene functions: Rv1876 - bacterioferritin BfrA; Rv1877 - MFS transporter; Rv1878 – gamma-glutamylpolyamine synthetase GlnA3, Rv1879 - hypothetical protein

365

366 **RNAseq analysis: Spermine upregulates the gene coding for the efflux pump**
367 **Rv3065**

368 To investigate which other factors were possibly regulated by spermine stress, we
369 compared the differences in gene expression of wild type *M. tuberculosis* with and
370 without spermine treatment. For six genes with median raw read counts greater 20, a
371 clearly reduced expression level with a log2 median fold change less than -3 was
372 determined. In contrast, for 13 genes with sufficient number of reads the expression was
373 increased by a log2 median fold change larger than 3 (Fig. 8).

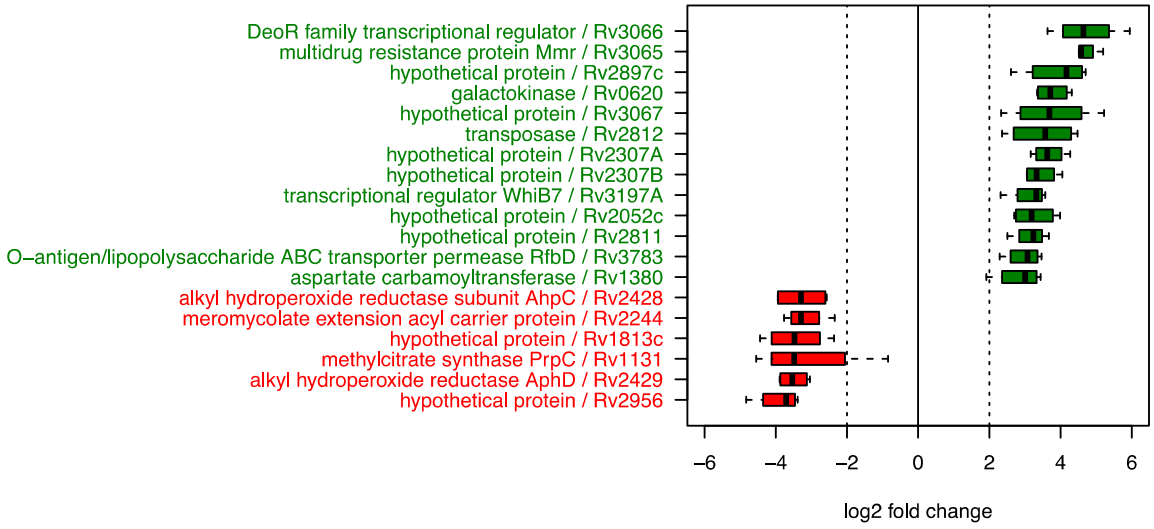

Fig. 8. Expression of genes altered upon spermine treatment of *Mycobacterium tuberculosis* wild type in 7H9 media. Shown are box plots obtained from 4 independent experiments.

374

375 Among the five genes found most prominently upregulated were *rv0620* (log2 median
376 fold change of 3.7; galactokinase) and *rv2897* (4.2 log2 fold; hypothetical protein), for
377 which no specific role in the infection process or in polyamine metabolism is known.
378 Interestingly, three other highly-upregulated genes (*rv3065, rv3066, rv3067*) are all
379 located within the same genetic locus, probably forming an operon. The gene *rv3065*
380 (log2 median fold change 4.6) codes for Mmr, a multidrug efflux pump that confers
381 resistance to tetraphenylphosphonium (TPP), erythromycin, ethidium bromide,
382 acriflavine, safranin O, pyronin Y and methyl viologen (41). The gene *rv3066* (log2
383 median fold change 4.6) codes for a putative transcriptional regulator of the DeoR
384 family, while *rv3067* (log2 median fold change 3.7) encodes an uncharacterized protein,

localised in the plasma membrane (https://www.uniprot.org/uniprotkb/I6YB21/entry). Bioinformatic analyses and previous studies (41) revealed that these proteins are neither found in *M. smegmatis* nor in *S. coelicolor.* Thus, it is tempting to speculate that Rv3065 is an important efflux pump, responsible for the excretion of polyamines and thus enabling *M. tuberculosis* to survive in excess spermine. Furthermore, in the model system *S. coelicolor*, a full transcriptome RNAseq analysis was performed in the presence of polyamines putrescine, cadaverine, spermidine and spermine in the wild type and in the *glnA3* mutant (17). This study supported our RNAseq results obtained in this work, and in connection with other experiments performed provided evidence that the second GlnA-like enzyme GlnA2 is involved in polyamine glutamylation. However, further investigation of this hypothesis was beyond the scope of this study.

3. MATERIALS AND METHODS

Strains and growth conditions.

M. tuberculosis (MTB) H37Rv was obtained from ATCC (27294) and genetically manipulated to obtain the mutant. The fluorescence expressing strain is an H37Rv strain carrying a shuttle vector (pCherry) (42, 43) expressing (under P_{smyc}) *m*Cherry (a variant of the *Discosoma sp* red fluorescent protein (D*s*Red) (44). Strains were cultured either in Difco Middlebrook 7H9 broth (Becton Dickinson, Heidelberg, Germany) supplemented with ADS (0.005 g/ml Bovine albumin fraction V, 0.002 g/ml dextrose, 0.85 mg/ml sodium chloride) containing 0.05% tyloxapol (Sigma Aldrich), 0.02% (v/v) glycerol, or OADC (0.05 mg/ml oleic acid, 0.005 g/ml Bovine albumin fraction V, 0.002 g/ml dextrose, 0.004 mg/ml catalase, 0.85 mg/ml sodium chloride), or cultured in the ready-made Sauton's media (HIMEDIA) containing glycerol (0.02%) and tyloxapol (0.05%). The solid media used for plating was 7H11 agar based (Sigma Aldrich) supplemented with either ADS or OADC. Spermine was obtained from Sigma Aldrich, and 100 mM stocks were made in DMSO and stored at -20°C for downstream experiments.

The parental strain *S. coelicolor* M145 as well as all mutants were incubated for 4-5 days at 30°C on the defined Evans-agar base (modified after (45) supplemented with following nitrogen sources: 50 mM ammonium chloride, 50 mM L-glutamine, 200 mM putrescine dihydrochloride, 25 mM spermidine trihydrochloride, and 25 mM spermine

tetrahydrochloride in appropriate concentrations. Genetic manipulation of *S. coelicolor* M145 was performed as described previously (46, 47).

419 Tab. 3. Strains and plasmids used in this study.
420

Strains	Genotype/Phenotype	Reference
E. coli NovaBlue	*rec*A1, *end*A1, *gyr*A96, *thi*-1, *hsdR*17 (rK12-, mK12+) *supE*44, *relA*1, *lac* [F', *pro*AB, *lacI*^{q}, *lacZ*ΔM15, Tn*10*] (Tet^{R})	Novagen
E. coli Novablue pRM4*glnA3*	NovaBlue with the plasmid pRM4*glnA3* (Km^{R})	(48)
E. coli XL1-Blue	*rec*A1, *end*A1, *gyr*A96, *thi*-1, *hsd*R17, *sup*E44, *rel*A1, *lac,* [F', *pro*AB, *lacI*^{q}Z_, M15Tn*10*, (Tet^{R})]	(49)
E. coli XL1-Blue pRM4-*glnA3*$_{Mt}$ S54D	XL1-Blue with the plasmid pRM4-*glnA3*$_{Mt}$ S54D	This work
E. coli XL1-Blue pRM4-*glnA3*$_{Mt}$ S199N	XL1-Blue with the plasmid pRM4-*glnA3*$_{Mt}$ S199N	This work
E. coli XL1-Blue pRM4-*glnA3*$_{Mt}$ N335L	XL1-Blue with the plasmid pRM4-*glnA3*$_{Mt}$ N335L	This work
E. coli S17-1	*recA*, *pro*, *mod*+, *res*−, *tra* genes from plasmid RP4 integrated in the chromosome, donor strain for conjugation	(50)
E. coli S17-1 pRM4 *glnA3*$_{Mt}$ S54D	S17-1 with the plasmid pRM4-*glnA3*$_{Mt}$ S54D, for conjugation with *S. coelicolor* M145	This work
E. coli S17-1 pRM4 *glnA3*$_{Mt}$ S199N	S17-1 with the plasmid pRM4-*glnA3*$_{Mt}$ S199N, for conjugation with *S. coelicolor* M145	This work
E. coli S17-1 pRM4 *glnA3*$_{Mt}$ N335L	S17-1 with the plasmid pRM4-*glnA3*$_{Mt}$ N335L, for conjugation with *S. coelicolor* M145	This work
E. coli S17-1 pRM4*glnA3*$_{Mt}$	S17-1, with plasmid pRM4*glnA3*$_{Mt}$ for conjugation with *S. coelicolor* M145	This work
E. coli BL21 (DE3) pLysS	F−, *ompT*, *hsdFB* (r$_{B}$−m$_{B}$−) *gal dcm* (DE3) pLysS (Cm^{R})	(51)
E. coli BL21 pET30*glnA3*$_{Mt}$	Bl21 (DE3) pLysS, over-expression of *glnA3*$_{Mt}$	This work
E. coli BL21 pET30*glnA3*$_{Mt}$S54D	BL21(DE3) with the plasmid pET30*glnA3*$_{Mt}$S54D	This work
E. coli BL21 pET30*glnA3*$_{Mt}$S199N	BL21(DE3) with the plasmid pET30*glnA3*$_{Mt}$S199N	This work
E. coli BL21 pET30*glnA3*$_{Mt}$N335L	BL21(DE3) with the plasmid pET30*glnA3*$_{Mt}$N335L	This work
S. coelicolor M145	*S. coelicolor A3(2)* without native plasmids: *spc1*$^{-}$ and *spc2*$^{-}$	(47)
S. coelicolor M145 Δ*glnA3*	*glnA3* mutant strain of *S. coelicolor* M145; insertional inactivation of *glnA3* by an *aac*(3)IV cassette, (Apr^{R})	(20)
S. coelicolor M145 Δ*glnA3* pRM4*glnA3*$_{Mt}$	*glnA3* mutant strain of *S. coelicolor* M145 with pRM4*glnA3*$_{Mt}$; (Apr^{R} and Km^{R})	This work
S. coelicolor M145 Δ*glnA3* pRM4*glnA3*$_{Mt}$S54D	*S. coelicolor* Δ*glnA3* with the plasmid pRM4*glnA3*$_{Mt}$S54D	This work
S. coelicolor M145 Δ*glnA3* pRM4*glnA3*$_{Mt}$S199N	*S. coelicolor* Δ*glnA3* with the plasmid pRM4*glnA3*$_{Mt}$S199N	This work

S. coelicolor M145 Δ*glnA3* pRM4*glnA3*$_{Mt}$N335L	*S. coelicolor* Δ*glnA3* with the plasmid pRM4*glnA3*$_{Mt}$N335L	This work
E. coli BL21 pYT/his-*glnA3*	pYT9 derivative for overexpression of His-*glnA3*$_{Sc}$	(16)
M. tuberculosis H37Rv	wild type	(54)
M. tuberculosis H37Rv Δ*glnA3*	*M. tuberculosis* derivative with deleted *glnA3* gene	This work
Plasmids		
pRM4	pSET152*ermE*p* with artificial RBS	(52)
pRM4*glnA3*	pRM4-derivative with *glnA3*$_{Sc}$ (*S. coelicolor*)	(48)
pRM4*glnA3*$_{Mt}$	pRM4-derivative with *glnA3*$_{Mt}$ (*M. tuberculosis*)	This work
pET30 Ek/LIC	ligation independent cloning (LIC), T7 Promoter, T7 transcription start, phage f1 origin of replication, detachable N-terminal His-tag and S-tag, C-terminal His-tag, T7 terminator, *lacI* coding sequence, pBR322 *ori*	Novagen
pET30*glnA3*$_{Mt}$	pET30-derivative with *glnA3*$_{Mt}$ (*M. tuberculosis*)	This work
pK18	pUC-derivative, *lacZ'α*-complementation system, Km^R	(53)

Growth curve and susceptibility testing of *M. tuberculosis*

Frozen stocks were used to inoculate starter cultures, after 7-10 days of incubation, these were used to sub-culture in various growth conditions, 7H9-ADS or Sauton's media, with and without spermine. For each tested concentration of spermine, a corresponding, untreated, DMSO control was included. The OD_{600} was measured and recorded every second day. To independently validate the data by fluorescence measurements *M. tuberculosis* growth was monitored using an mCherry expressing *M. tuberculosis* H37Rv strain which was analyzed at various time points, in a 96-well dark plate, using a multimode plate reader (Synergy 2, Biotek/Agilent) (55). The minimum inhibitory concentration (MIC) was also determined with the broth-microdilution method, using resazurin to enable colorful detection of growth as previously described (56, 57). In order to evaluate the susceptibility of the strains by CFUs count, logarithmic phase cultures, were adjusted to an OD_{600} of 0.2, this then was diluted 100X, to have approximately 10^4 CFUs/ml, and this was then exposed to either 2 mM spermine or the

436 DMSO-control for about 3 hours in a 96-well plate, at 37°C. These were serially diluted
437 and plated on solid media that were incubated for up to 3 weeks. The CFUs of the
438 treated culture was divided by the CFUs of the untreated DMSO control culture, in order
439 to determine the percentage survival, this was repeated at least 8 times.
440
441 **Generation and complementation of the *M. tuberculosis* Δ*glnA3* mutant**

442 This was achieved as previously described (36, 37). Briefly, approximately 2500 bp
443 fragments upstream (US) and downstream (DS) *rv1878* (*glnA3*) were amplified using pfu
444 high fidelity GC rich target polymerase (Agilent) primers listed in Table 3. These were
445 subsequently cloned into the pJET sub-clonig vector (CloneJET PCR Cloning Kit,
446 Thermofischer). Then the US and DS fragments were restricted using enzymes *Bsr*GI,
447 S*pe*I and *Hin*dIII, which were incorporated in the primer design (see Table 3). Using a
448 two-way ligation method, the restricted US and DS fragments were ligated to the p2NIL
449 suicide plasmid (36), previously linearized with *Bsr*GI and *Hin*dIII. Then the *Pac*I
450 restriction fragment containing, *lacZ*, and *sacB* genes was restricted from pGOAL17 (36)
451 and cloned into the *Pac*I site of p2NIL. The phage resistant and endonuclease I (*endA1*)
452 deficient *E. coli* strain D10-beta (New England Biolabs Inc.) was used in the entire
453 cloning process. The integrity of the inserts was verified by Sanger sequencing at the
454 end of each cloning step, throughout the cloning process (sequencing primers found in
455 Table 3). The resulting construct p2NIL-A3-US/DS-G17, was used to transform *M.*
456 *tuberculosis*, and the mutant was generated through two subsequent homologous
457 recombination events as previously described (36). The mutant was screened by PCR
458 (primers in Table 3), confirmed by Southern blotting as previously described (37) and by
459 targeted genome sequencing (58). The mutant was complemented as previously
460 described (37), using the pMVhsp60 integrative vector (59), where *glnA3* was cloned
461 downstream the heat shock promoter (P_{hsp60}), to maintain constitutive expression at 37°C
462 (Table 3).
463
464 Table 4. Primers used in the study

Primer	Sequence	RS*	Purpose	Product/ size
A3-USF	GCTGTACATCTCAAGCCAGGAATCGT	Bsr	In frame deletion of 1245 bp of the 1353 bp of	US= 2402 bp

	CAT	gI	*rv1878*	
A3-USR	GCACTAGTCAAGCGGTGTGGCTGTCAT	SpeI		
A3-DSF	GCACTAGTTCGCGGTACGCCAGTTAGA	SpeI		DS= 2404 bp
A3-DSR	GCAAGCTTAACCGCGCCAACTACCTGAC	HindIII		
A3-SF	GGTCGACTCCCTCGCAGTTT	NA	Screening of deletion mutants	
A3-SR1	CGATCCGGCTCAGTGTTCC	NA		**Set 1:** WT= **614bp** **Δ = 0 bp** **Set 2:** WT=**2251bp** Δ = 2251-1245= **1006bp**
A3-SR2	GCAGCAGAACCCGATCCTGT	NA		
A3-F	AAGCTTAGAAGGAGAAGTACCGATGACAGCCACACCGCTTG	HindIII	Complementation of Δ*rv*1878	1383+16+6+8=1413
A3-R	GCGTTAACTTACACACTCCAAGCCATCCGG	HpaI		
G17-NIL-DS-R	GTGCCTGACTGCGTTAGCAA	NA	Sequencing the final construct	5000-6000bp Flanking outside inserted US and DS
NIL-LACZ-US-F1	GCACCGCCGAAACCCTTAT	NA	Sequencing the final construct	
NIL-SACB-US-F2	GGCTGCAGGAATTCGATATCA	NA	Sequencing the final construct	
A3-Seq-R	AACGATGGTTTGGCCGGT		Sequencing inserts of the *rv1878* deletion construct The homologous recombination template	
A3-Seq-F1	GCCAGGAATCGTCATGTGC			
A3-Seq-F2	CAGCACCGTTGACCAGTCGT			
A3-Seq-F3	CAGTGGCGCTGGGTTTCTT			
A3-Seq-F4	AGTGCCATCTCCGGCTGTCT			
A3-Seq-F5	TTGAAGCGACAGCCAGACC			
A3-Seq-F6	TTGATCCGCAGACTTATTGGG			
A3-Seq-F7	AATCGTGTTGCTGCACTGCT			
A3-Seq-F8	CGTTCGATGTCAAAGCGGT			
A3-Seq-F9	CCTACGACGTCCACAATCCC			
78-seq-3	GCATCGCTATCGAGCAGTT		Sequencing of insert in *rv1878* complementation construct (primers MV-F	
78-seq-4	GGAATCTATGCATGCTGGG			

			and SR-1 were used as well)	
Reverse transcriptase PCR primers and probes				
Primer	**Sequence**	**Probe**	**Sequence (5'-Fam/ 3'-quencher)**	**Purpose**
16S-RT-F	GACCACGGGATGCATGTC	16S-probe	CACCCCACCAACAAGCTGATAGGC	Housekeeping gene to normalise RT-PCR data of each gene
16S-RT-R	CCGTCGTCGCCTTGGTAG			
76-RT-F	GCTATCAACCAATACTTTCTGCACT	76-probe	TCGACGAAATGCGGCACG	Quantification of the expression level of *Rv1876*
76-RT-R	ATCCAGCAACAAGATGCGA			
77-RT-F	GCTGTACCTGGTCGTCCT	77-probe	TGTTCTGCACGATGAGAACGAGCCAC	Quantification of the expression level of *Rv1877*
77-RT-R	AAGGTCACACCCGATGTTG			
78-RT-F	GATACGCCGGACCAACACA	78-probe	ATCCTGGCCTCGGCGCCA	Quantification of the expression level of *Rv1878*
78-RT-R	ACAGAAGGTATGCCACACCG			
79-RT-F	CGACTGGCTGGTGGAG	79-probe	TCGTGAGCGTGGCTGCCCG	Quantification of the expression level of *Rv1879*
79-RT-R	GGCGCAGTATCTCGTTG			
ovglnA3mtF	GACGACGACAAGATGACAGCCACACCGCTTGC			Amplification of the gene $glnA3_{Mt}$ of *M. tuberculosis* H37Rv for pET30 vector
ovglnA3mtR	GAGGAGAAGCCCGGTTACACACTCCAA GCCAT			Amplification of the gene $glnA3_{Mt}$ of *M. tuberculosis* H37Rv for pET30 vector
Km1	GACAGGATGAGGATCGTTTC			
Km2	AATCTCGTGATGGCAGGTTG			
T7	TAATACGACTCACTATAGGG		Eurofins Scientific SE	Sequencing of insert in pET30*glnA3*$_{Mt}$
T7 term	CTAGTTATTGCTCAGCGGT		Eurofins Scientific SE	Sequencing of insert in pET30*glnA3*

				$_{Mt}$
CglnA3mt-F	CGCCCATATGACAGCCACACCGC			Amplification of the gene *glnA3*$_{Mt}$ of *M. tuberculosis* H37Rv for pRM4 vector
CglnA3mt-R	TCCAAGCTTTTACACACTCCAAGCCA			Amplification of the gene *glnA3*$_{Mt}$ of *M. tuberculosis* H37Rv for pRM4 vector
glnA3mtmut4F	GGCGCCAACCCGGTGTGGCATACCTTC TGTATCGAC			
glnA3mtmut4R	CACCGGGTTGGCGCCGAGGCCAGGATTGGCGAATGT			
glnA3mtmut5F	GAGATCAACTTAGCGCCGCAGCCGCCGGTCGCGGCC			
glnA3mtmut5R	CGCTAAGTTGATCTCGAATTGGTTGGCACCGTATTC			
glnA3mtmut6F	GGCGGGCTCGTGGAGGTGAAGGTCGTCGACCCGTCG			
glnA3mtmut6R	CTCCATGAGCCCGCCGTACGCGCTGCCAGCCCCGCC			
hrdB-qrt1	TGACCAGATTCCGGCCACTC			PCR-primer for housekeeping gene *hrdB* (control)
hrdB-qrt2	CTTCGCTGCGACGCTCTTTC			PCR-primer for housekeeping gene *hrdB* (control)
M13 uni (-21)	TGTAAAACGACGGCCAGT			Sequencing of insert in pRM4*glnA3*$_{Mt}$
M13 rev (-49)	GAGCGGATAACAATTTCACACAGG			Sequencing of insert in pRM4*glnA3*$_{Mt}$
pRM_GenF	CTGCAAGGCGATTAAGTTGG			Sequencing of insert in pRM4*glnA3*$_{Mt}$
pRM_GenR	TTATGCTTCCGGCTCGTATG			Sequencing of insert in pRM4*glnA3*$_{Mt}$

Complementation of the *S. coelicolor* Δ*glnA3* mutant.

For complementation of the *S. coelicolor* $glnA3_{Sc}$ mutant, the $glnA3_{Mt}$ gene from *M. tuberculosis* was amplified by PCR using *CglnA3mtF* and *CglnA3mtR* primers and cloned into the multiple cloning site of pRM4 plasmid between *Nde*I and *Hin*dIII restriction sites downstream of the constitutively expressed erythromycin promoter *ermE*p* located on the plasmid. The kanamycin resistance cassette was amplified by PCR using the pK18 plasmid as a template and primers *aphIIupperEcoR*I as well as *aphIIlowerHind*III, and introduced to the multiple cloning site of the recombinant plasmid pRM4-*glnA3MtC* between *Eco*RI and *Hin*dIII restriction sites. The correct construct was confirmed by colony PCR as well as by sequencing and introduced into the *S. coelicolor* $glnA3_{Sc}$ mutant by biparental conjugation using *E. coli* S-17. Clones were selected on resistant phenotype against kanamycin and apramycin. The correct integration of the pRM4-*glnA3Mt* was confirmed by PCR and sequencing.

Cloning, expression, and purification of His-Strep-GlnA3$_{Mt}$

The $GlnA3_{Mt}$ encoding gene *Rv1878* was amplified using genomic DNA of *M. tuberculosis* as template. It was inserted into the expression vector pET-30 Ek/LIC (Novagen) under the control of the IPTG inducible T7 promoter using the pET-30 Ek/LIC Cloning Kit (Novagen). His/Strep-$GlnA3_{Mt}$ was synthesized in *E. coli* BL21 (DE3). Initially cells were incubated over night at 37˚C in LB medium, afterwards transferred in fresh LB medium and incubated for at 25˚C until the culture reached an optical density of 0.5 at 600 nm. Subsequently, the culture was induced with 1 mM IPTG and incubated at 25˚C overnight. His/Strep-$GlnA3_{Mt}$ was purified by nickel ion affinity chromatography essentially as directed by the resin manufacturer (GE-Healthcare). Purified His/Strep-$GlnA3_{Mt}$ was dialyzed against 20 mM Tris, 100 mM NaCl (pH 8.0) or used for further purification steps. His/Strep-Tag was cleaved using enterokinase according to the protocol of the manufacturer (NEB) and $GlnA3_{Mt}$ was immediately purified from the digestion mix by size-exclusion chromatography as directed by the resin manufacturer (GE-Healthcare).

HPLC/ESI-MS detection of a glutamylated product

For the detection of the glutamylated product of the $GlnA3_{Mt}$ catalyzed reaction, an HPLC/ESI-MS procedure has been applied. Standard reactions contained: 20 mM

HEPES (pH 7.2), 10 mM ATP, 150 mM glutamate sodium monohydrate, 150 mM putrescine dihydrochloride, cadaverine dihydrochloride, spermidine trihydrochloride, or spermine tetrahydrochloride, 20 mM $MgCl_2x6H_2O$, were mixed with 10 µg of the purified His/Strep-$GlnA3_{Mt}$ or $GlnA3_{Mt}$ (or without GlnA3 as a control) and incubated at 30˚C for 5 min. The reaction mixture was incubated at 100˚C for 5 min in order to stop the reaction. HPLC/ESI-MS analysis was performed on an Agilent 1200 HPLC series using a Reprosil 120 C_{18} AQ column, 5 µm, 200 mm by 2 mm fitted with a precolumn 10 mm by 2 mm (Dr. Maisch GmbH, Ammerbuch, Germany) coupled to an Agilent LC/MSD Ultra Trap System XCT 6330 (Agilent, Waldbronn, Germany). For analysis were used: 0.1% formic acid as solvent A and acetonitrile with 0.06% formic acid as solvent B at a flow rate of 0.4 ml min^{-1}. The gradient was as follows: $t_0 = t_5 = 0\%$ B, $t_{20} = 40\%$ B (time in minutes). Injection volume was 2.5 µl, column temperature was 40˚C. ESI ionization was done in positive mode with a capillary voltage of 3.5 kV and a drying gas temperature of 350˚C.

Modified GS activity assay

The enzymatic activity of $GlnA3_{Mt}$ variants was tested in a modified GS activity assay(24). Solutions A, B, C and F and the reaction mix were prepared containing enough protein for the release of 35-50 mM Pi produced in 5 min. After the adjustment of the pH, 95 µl were loaded into PCR-strips for each reaction. Solution D or Solution E for undetermined kinetic parameters of ATP was prepared. Afterwards, the reaction was initiated by adding 5 µl substrate to the reaction mix. Additionally, blanks with H_2O_{deion} and a phosphate standard ranging from 0 to 20 mM were included. The reaction mix was incubated at 30°C for 5 min in a thermocycler. The wells of a 96-well plate were loaded with 150 µl of solution D (or C) for each reaction. Afterwards, 50 µl of the reaction mix was transferred to the previously prepared solution D (or C) in the 96-well plate. Solutions were mixed and incubated for 5 min at RT. At low pH the enzymatic reaction was terminated, while 150 µl of solution F were added to stop color development. The final reaction was incubated for 15 min at RT. The absorbance was measured at 655 nm using a Microplate reader. Raw absorbance readings were put into Excel (Microsoft).

***In silico* protein modeling and docking studies**

To build the *in silico* models for the different GlnA-like enzymes an existing template from the Protein Data Bank (PDB) was selected. The initial template search was done using the template search function of SWISS-MODEL (25) by input of the amino acid sequence in FASTA format, plain text or UniProtKB accession code. SWISS-MODEL was then performing search for evolutionary related protein structures against the SWISS-MODEL template library SMTL (60) and using database search methods BLAST, and HHblits (61, 62). The resulting template structures were ranked and further evaluated by SWISS-MODEL using the estimated Global Model Quality Estimate (GMQE) (60) and the Quaternary Structure Quality Estimate (QSQE) (63). Top-ranked templates and alignments were compared to verify whether they represent alternative conformational states or cover different regions of the target protein. In such case, multiple templates were selected automatically and different models were built accordingly (25). Out of the resulting list of possible templates different templates were chosen based on the GMQE, QSQE, identity and oligo state. Also, value was given to select templates out of different bacterial phyla to get quality control with diversity. Using the selected templates as a base SWISS-MODEL built a 3D protein model estimating the real 3D structure of the protein. Therefore, SWISS-MODEL started with the conserved atom coordinates defined by the target-template alignment and then coordinated residues corresponding to insertions/deletions in the alignment that were generated by loop modelling and a full-atom protein model was obtained by constructing the non-conserved amino acid side chains (25). SWISS-MODEL used the ProMod3 modelling engine and the OpenStructure computational structural biology framework (64). The evaluation of the build 3D protein models was done using the QMEAN scoring function, the MolProbity score and a Ramachandran plot of the model. The QMEAN score provided an estimate of the ‘degree of nativeness’ of the structural features observed in a model and described the likelihood that a given model was of comparable quality compared to experimental structures (31). The MolProbility score relied heavily on the power and sensitivity provided by optimized hydrogen placement and all-atom contact analysis, complemented by updated versions of covalent-geometry and torsion-angle criteria (33). The Ramachandran plot plotted the torsion angles of the different amino acids against each other to verify the correct folding of the *in silico* model (32). Based on the highest QMEAN score and the Ramachandran plot the best *in silico* 3D

protein models were chosen. Molecule structures were obtained from the PubChem database. Molecular docking was performed using UCSF Chimera software.

Site directed mutagenesis

To select possible key amino acids the *in silico* 3D structures of $GlnA3_{Mt}$ were compared with the template structures they originate from. The main used 3D model of the $GlnA3_{Mt}$ enzyme was based on the GlnA1 (PDB code 1HTO) structure of *M. tuberculosis* (26). Therefore, the 3D structure model of $GlnA3_{Mt}$ and the template structure were opened with SWISS-PDB viewer (65), PyMol (PyMOL, The PyMOL Molecular Graphics System, Version 2.0 Schrödinger, LLC.) or UCSF Chimera. Through literature research key amino acids, of the template, could be identified and then marked in the 3D template structure. The amino acids that overlap directly with the key amino acids of the template were marked. The used site-directed mutagenesis approach was based on the protocol described by Zheng et al. (66). It was using a PCR approach with specifically designed primers to induce into plasmid DNA. The primers contained the wanted mutation with was introduced in the plasmid DNA through the PCR amplification. The $GlnA3_{Mt}$* mutated variants were generated using the pET-30 Ek/LIC plasmid with the cloned *glnA3* gene as template and were expressed in *E. coli* strain BL21 (DE3).

RNA sample preparation

A volume of 10 ml of early to mid-logarithmic phase cultures was either treated with spermine or the DMSO control, and harvested 3 hours later using the RNA Pro Blue kit (MP Bio), and the resuspended cells were homogenised using the Fast Prep Homogenizer (30 seconds, 6 m/s, four times, 5 min intermittent). The cell lysate was filtered twice using PTFE syringe filters (13 mm diameter, 0.2 µM pores size) and taken out of the BSL3 laboratory for further purifications. The first purification was performed using the Direct-zol RNA Miniprep Plus (R2070, 100 µg binding capacity) including an in-column DNA digestion step, according to the manufacturer's instructions. The purified samples were quantified using a spectrophotometer, and diluted if the concentration exceeded 200 ng/µl. Then they were further digested using the Turbo DNA-free kit

(Thermofischer) according to manufacturer's instructions, however in two consecutive rounds, to ensure complete DNA digestion. The digested samples were further purified and concentrated using the RNA clean and concentrator kit-25 (R1017, 50 µg binding capacity), including another in-column DNA digestion step, according to manufacturer's instruction. The resulting samples were used for Next Generation RNA sequencing performed by Eurofins Genomics GmbH.

RNA sequencing

Bulk RNA sequencing of the resulting samples as well as expression quantification was performed by Eurofins Genomics GmbH. RNA quality was measured using the Agilent 2100 Bioanalyzer and all but one sample had RIN value larger 8. Sequencing was performed on the Illumina Novaseq 6000 using the NEBNext(R) Ultra II Directional RNA Library Prep Kit, generating between 13.5 and 17.3 million 150-bp paired-end read pairs. Reads were mapped to the genome sequence of Mycobacterium tuberculosis H37Rv (NC_000962.3; obtained from https://www.ncbi.nlm.nih.gov/nuccore/NC_000962.3?report=fasta) using bwa-mem version 0.7.12-r1039 (67). With the exception of one sample with 89% of reads mapping to H37Rv, all samples had a mapping rate larger than 97%. Reads were subsequently counted for 3,906 *Mycobacterium tuberculosis* H37Rv genes according to RefSeq annotation (obtained via https://www.ncbi.nlm.nih.gov/Taxonomy/Browser/wwwtax.cgi?id=83332) using tool featureCounts (68). Raw overall read counts per sample are between 4.4 and 8.8 million (counting each read pair once and omitting multi-mapping and low-quality reads). Trimmed mean of M-values (TMM) normalization (69) of raw counts was performed using the edgeR package version 3.16.5 (70). In a multidimensional scaling plot, the first dimension separated spermidine-treated from untreated samples. Normalized counts were used for computation of fold changes and computation of median fold changes, which were log2 transformed whenever specifically noted.

RT-PCR

In order to perform the reverse-transcriptase quantitative PCR, (RT-PCR), RNA samples were converted to cDNA using the Maxima First Strand cDNA KIT (Thermofischer). During method optimization, controls where all reagent were added except the reverse transcriptase were included (non-reverse transcriptase control), in order to run it along

with the converted samples, to ensure that genomic DNA was completely removed or negligible. The reverse transcribed samples were run in a 10 µl reaction on a LightCycler 480, using the LightCycler 480 master mix. Quantification was made by the integrated software of the LightCycler, according to a probe-based assay (labelled at the 5'-end with FAM and at the 3'-end with a quencher), using *M. tuberculosis* genomic DNA to generate a standard curve (10-1000 pg/µl). The probe and primers were designed by TIB MOLBIOL Syntheselabor GmbH. Various set of primers were designed, and these were tested, to obtain the optimal set, that was used for the quantification (Table 3).

4. DISCUSSION

During evolution, many intracellular pathogens (including protozoan parasites) have developed strategies to access selected nutrients from the host for their growth and survival. *M. tuberculosis* is an example of an intracellular pathogen, which is very well adapted to survive within the hostile macrophage environment. The long term host and pathogen persistence is the consequence of a subtle equilibrium between the nutritive needs of host and pathogens. On one hand, the presence of high polyamine levels in the M2 intracellular environment of macrophages may lead to growth inhibition or cell death of *M. tuberculosis* (71). Already 70 years ago it was reported that polyamines like spermine show a tuberculostatic activity (72). On the other hand, polyamines may provide a nutrient source that can be exploited by *M. tuberculosis*.

Since free spermine is toxic to cells, it has to be immediately excreted or metabolized further and neutralized by a modification such as acetylation (73) or gamma glutamylation (16, 18). The modified spermine is no longer toxic for bacteria due to loss of its positive charge (74). Glutamylated spermine may be subsequently utilized as N/C-source or excreted from cells.

In order to investigate how *M. tuberculosis* can survive under excess polyamine we took advantage of the knowledge on polyamine metabolism in *S. coelicolor,* which is a model actinobacterium that shares essential features in nitrogen metabolism with *M. tuberculosis*. The gamma-glutamylpolyamine synthetase $GlnA3_{Sc}$ is the primary enzyme of the polyamine utilization pathway in *S. coelicolor* (16) catalyzing the first step of polyamine utilization, the detoxification of polyamine by glutamylation. Thus, we hypothesized that a similar polyamine utilization pathway might enable pathogenic

actinobacteria, such as *M. tuberculosis*, to colonize host cells and evade the host's immune response by conferring resistance against toxic polyamines and ensuring putative polyamine utilization necessary for long-term persistence. Transcription of *glnA3*$_{Mt}$, the mycobacterial orthologue of *glnA3*$_{Sc}$, was reported in broth culture (75) and the respective protein was detected in a guinea pig model of tuberculosis *in vivo*, during the chronic stage of this disease (76, 77). *glnA3*$_{Mt}$ was reported to be poorly expressed in *M. tuberculosis* under laboratory conditions (19). Its presence in the cell is not essential for bacterial homeostasis, however its role was not evaluated in the presence of high polyamines concentrations reflecting disease relevant conditions.

In the current study we observed that *M. tuberculosis* growth can be inhibited by spermine. Using a GS-based *in vitro* enzymatic activity assay we show that GlnA3$_{Mt}$ (Rv1878) acts as a gamma-glutamylspermine synthetase and generates a glutamylated spermine. In an *in vitro* phosphate release assay we demonstrated that purified recombinant GlnA3$_{Mt}$ prefers spermine as a substrate, over putrescine, cadaverine, spermidine or other monoamines and amino acids. These results lead to the conclusion that GlnA3$_{Mt}$ may play a specific role in the detoxification of the polyamine spermine. We therefore speculated that GlnA3$_{Mt}$ may be essential for the survival of *M. tuberculosis* during spermine stress. However, the deletion of the *glnA3* gene in *M. tuberculosis* did not result in immediate death of the bacteria or a reduced growth rate of the strain in the presence of high spermine concentrations. Thus, at the moment, the specific functional role of GlnA3$_{Mt}$ in *M. tuberculosis* remains unclear. The assumption that GlnA3 may play a detoxifying role only at rather low spermine levels could be excluded since a similar growth rate of WT and *glnA3*-deficient *M. tuberculosis* was observed at all spermine concentrations tested.

A further finding that GlnA3$_{Mt}$ is probably not crucial for survival under polyamine stress was obtained from transcriptional analyses: The *gln*A3$_{Mt}$ gene is part of a locus consisting of four genes, comprising (*rv1876*) – encoding bacterioferritin A (*bfrA*) (77), *rv1877* – encoding a multidrug efflux pump (40), *glnA3* (*rv1878*) - gamma glutamyspermine synthetase, and *rv1879* – encoding a putative amidohydrolase. Both RNAseq analyses and subsequent confirmatory RT-PCR showed that the gene cluster *rv1876-rv1877-rv1878-rv1879* was not upregulated in the presence of spermine,

suggesting that $GlnA3_{Mt}$ does not participate in a spermine-induced transcriptional response in this bacterium.

In contrast, RNAseq revealed three alternative genes to be significantly upregulated in response to spermine: *rv3065*, *rv3066*, and *rv3067*. Interestingly, *rv3065* encodes an efflux pump suggesting that active excretion of polyamines is the bacterium's primary defence against this class of molecules. Rv3065 was the first mycobacterial protein identified and described in the small membrane protein family (SMR) in *M. tuberculosis* (78). This represents a group of efflux pumps that contain four transmembrane domains and confer resistance to aromatic dyes, derivatives of tetraphenylphosphonium (TPP) and quaternary amines (79). Rv3065 has independently been shown to mediate the efflux of different chemical compounds and antibiotics belonging to the pyrrole and pyrazolone chemical classes (80). Over-expression of *rv3065* in *M. tuberculosis (*81) and in *M. smegmatis* (78) increased resistance to to tetraphenylphosphonium (TPP), erythromycin, ethidium bromide, acriflavine, safranin O, and pyronin Y.

Of note, joint transcription of *rv3065-rv3067* has previously been observed in *M. tuberculosis* treated with thioridazine (80). Thus, it is possible that spermine may also be a substrate for Rv3065. We have also seen that *rv1877*, encoding for another efflux pump was up-regulated during spermine stress in 7H9 medium, thereby pointing also to a particular role of efflux activities. Such a resistance mechanism would make the detoxification of spermine superfluous and could explain the survival of the *glnA3Mt* mutant in the presence of spermine

Conclusion

In this study, the enzymatic function of $GlnA3_{Mt}$ and the anti-mycobacterial activity of spermine were demonstrated. However, further studies are needed to decipher the spermine detoxification mechanisms in *M. tuberculosis*. In particular, an interplay of GlnA3 and the second gamma-glutamylpolyamine synthetase GlnA2 as well as potential polyamine transporter Rv3065 seems to compose a complex system to escape spermine toxicity by *M. tuberculosis*.

5. ACKNOWLEDGEMENTS

We acknowledge support by the Federal Ministry of Education and Science (Bundesministerium für Bildung und Forschung - BMBF) and cooperation partners from

the GPS-TBT and GSS-TUBTAR projects as well as the DZIF projects within TTU-TB "New drugs and regimens" and the TTU-NAB "Novel Antibiotics". WW acknowledges infrastructural funding from the Cluster of Excellence EXC2124 (Controlling Microbes to Fight Infection, project ID 390838134) from the DFG. We gratefully acknowledge Carolin Golin (Borstel) and Alena Strüder (Tübingen) for expert technical assistance and Dr. Gareth Prosser (Borstel) for helpful suggestions and critical reading of the manuscript. We acknowledge support by Open Access Publishing Fund of University of Tübingen.

6. FUNDING

This research was funded by the Federal Ministry of Education and Science BMBF (Fördermaßnahme "Targetvalidierung für die pharmazeutische Wirkstoffentwicklung"), project GPS-TBT (FKZ: 16GW0183K, 16GW0184) as well as project GSS-TUBTAR (FKZ: 16GW0253K, 16GW0254).

7. CONFLICT OF INTERESTS

All authors declare no conflict of interest.

8. AUTOR CONTRIBUTIONS

AM, WW, NR, DH, CSE, FH, SK designed the study and developed the methodology. SK and MO cloned, overexpressed and purified the GlnA3$_{Mt}$ protein. SK and MB cloned, overexpressed and purified the His-Strep-GlnA3$_{Mt}$* protein variants. SK and MO constructed and analyzed the *ΔglnA3*$_{Sc}$pRM4*glnA3*$_{Mt}$ complementation strain. SK analyzed DNA/protein sequences, protein structures, molecular docking data, HPLC, MS/MS and assay data. CSE generated the *M. tuberculosis glnA3* mutant, prepared *M. tuberculosis* samples, performed survival assays, carried out RT-PCR analysis and prepared and managed RNAseq samples and results. IW investigated RNA-Seq data analyses and computed and visualized expression changes. SK, CSE, NR wrote the manuscript. SK and MB performed homology modeling of proteins. SK, MO and MB performed phenotypical analysis of all mutants and parental strain *S. coelicolor* M145 on Evans medium with different nitrogen sources. CM cloned, overexpressed and purified SUMO-GlnA3$_{Mt}$* protein variant. SK, MB, and CM performed GlnA3$_{Mt}$ *in vitro* assay. AK performed the HPLC and HPLC/MS analyses. WW, NR, DH, CSE, FH, HBO provided

helpful feedback on an early draft of the paper and assisted with data analysis. SK, MO, MB, NR and CM prepared all figures for manuscript. SK, CM, AM, AK, WW, NR, DH, FH, and IW contributed to the editing of the manuscript and resolved final approval of the version to be published.

Supplementary figures

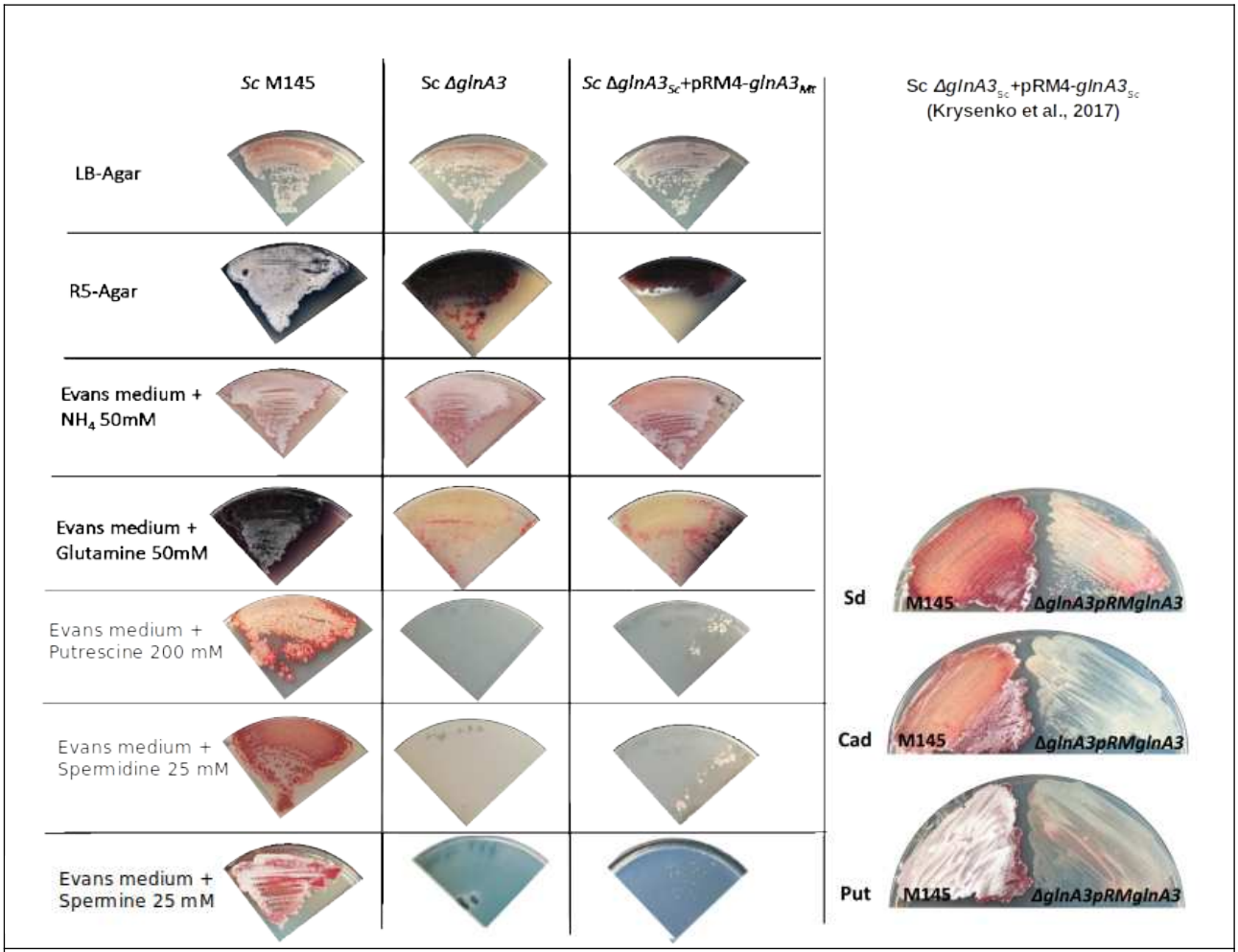

Suppl. Fig. 1. Physiological role of the $glnA3_{Mt}$ gene product in the *S. coelicolor glnA3* mutant grown in the presence of polyamines and other nitrogen sources. Phenotypic comparison of the parental strain *S. coelicolor* M145, the *glnA3* mutant and the *ΔglnA3Sc*pRM4$glnA3_{Mt}$ complementation strain grown on rich LB-agar, R5-agar or defined Evans medium supplemented with glutamine (50 mM), NH_4Cl – ammonium chloride (50 mM) and polyamines putrescine (200 mM), spermidine or spermine (25 mM) as sole nitrogen source. Each panel represents observations on a single agar plate. Complementation of the *S. coelicolor glnA3* mutant with $glnA3_{Mt}$ resulted in restored growth of the strain in the presence of high putrescine, spermidine and spermine concentrations.

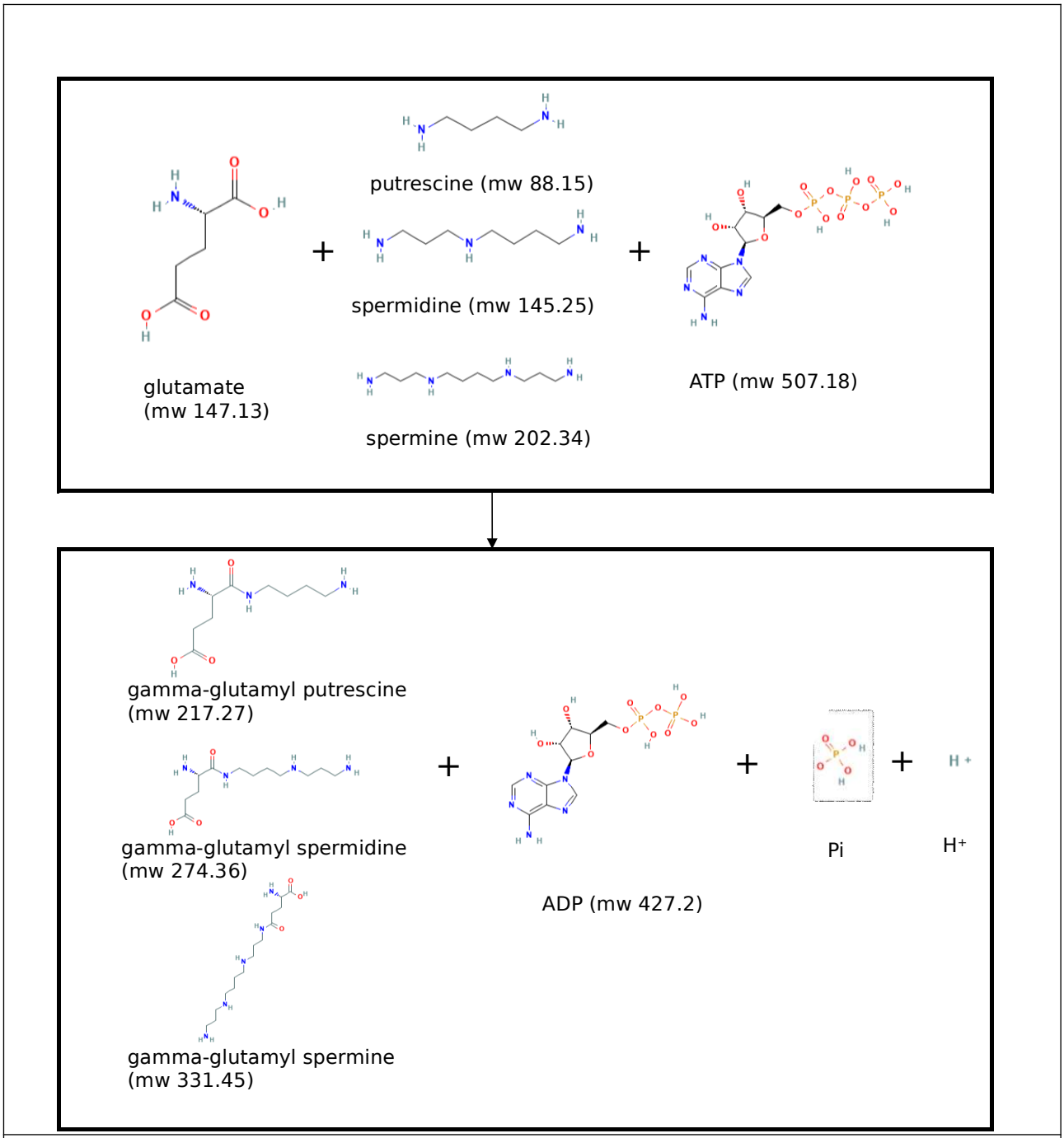

Suppl. Fig. 2. Reaction catalyzed by gamma-glutamylpolyamine synthetase with indicated substrates, products and molecular weight of each molecule.

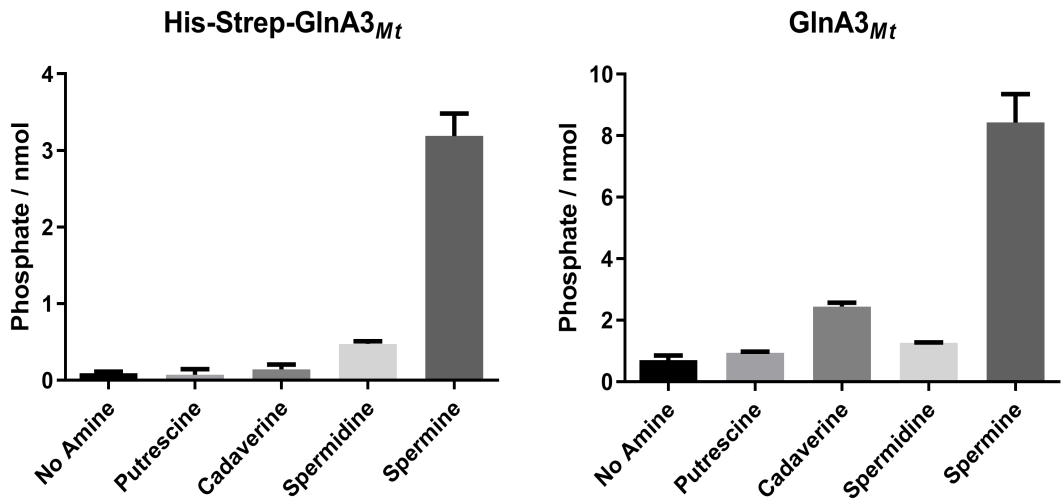

Suppl. Fig. 3. Specific activity of the native $GlnA3_{Mt}$ with different polyamines. All substrates are at a concentration of 50 mM. The mean value of minimum n=3 biological replicates with n=3 technical replicates each with standard error is shown.

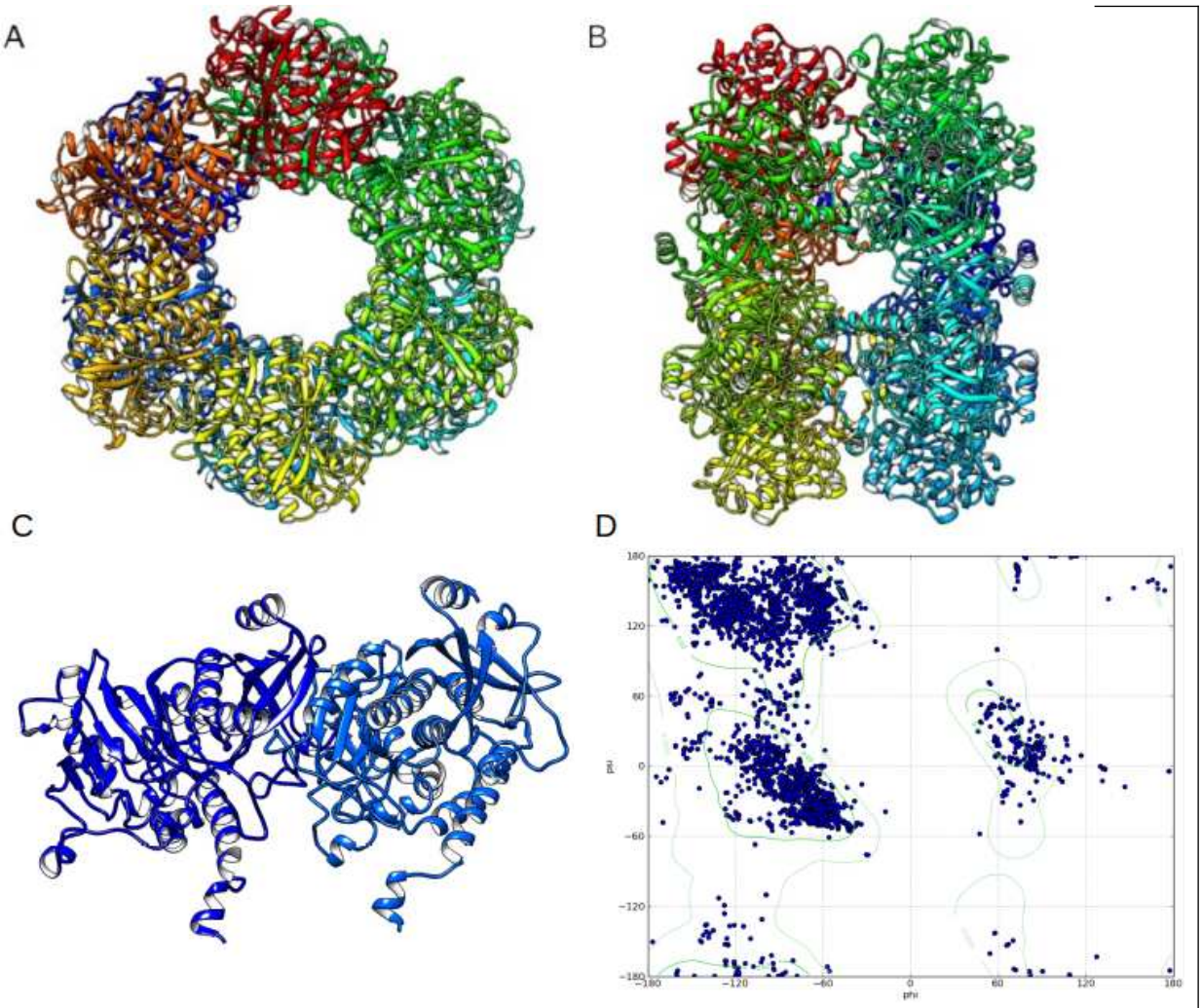

Suppl. Fig. 4. Structural alignment of the 3D model structure of $GlnA3_{Mt}$, based on and superposed with the $GlnA_{Mt}$ template (PDB code 1BVC (27)). A) each of the twelve subunits is marked in a different color (color scheme “chain”), B) side-view on two 6-unit containing rings, C) a representation of the active site and substrate binding pocket, D) Ramachandran plot demonstrating the good quality of the generated $GlnA3_{Mt}$ model, based on visualization of energetically allowed regions for backbone dihedral angles ψ against φ of amino acid residues in the structure.

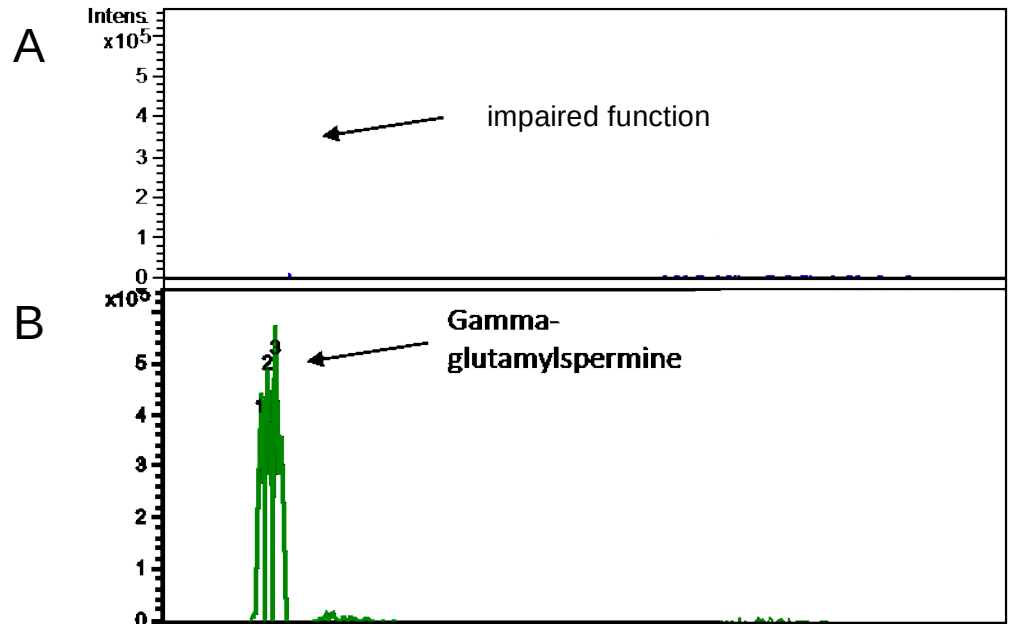

Suppl. Fig. 5. HPLC/ESI-MS analysis of His-Strep-GlnA3$_{Mt}$SER199 and His-Strep-GlnA3$_{Mt}$. Two samples were analyzed in MS negative mode: reaction mixtures with addition of His-Strep-GlnA3$_{Mt}$SER199 (A) and with addition of His-Strep-GlnA3$_{Mt}$ (B). Extracted ion chromatograms for the His-Strep-GlnA3$_{Mt}$ reaction product corresponding to gamma-glutamylspermine with charge to mass ratio of *m/z* 331 was shown (B), and no product in the sample with GlnA3$_{Mt}$SER199 was detected (A).

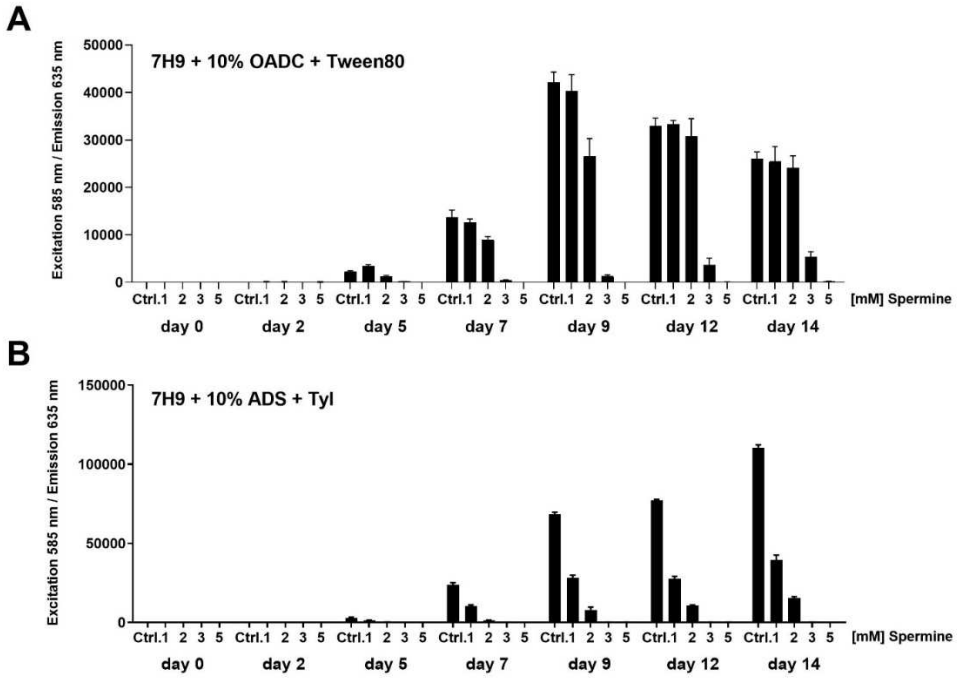

Suppl. Fig. 6. Growth of *M. tuberculosis* in the presence of spermine. *m*Cherry10- expressing Mtb H37Rv bacteria (55) were incubated for a period of 14 days in the absence or presence of spermine in (A) 7H9 medium + OADC + Tween80 or (B) in 7H9 medium + ADS + Tyloxapol and analyzed as described (55); Ctrl: DMSO; Spm: spermine. Concentrations tested were from 1mM to 5 mM.

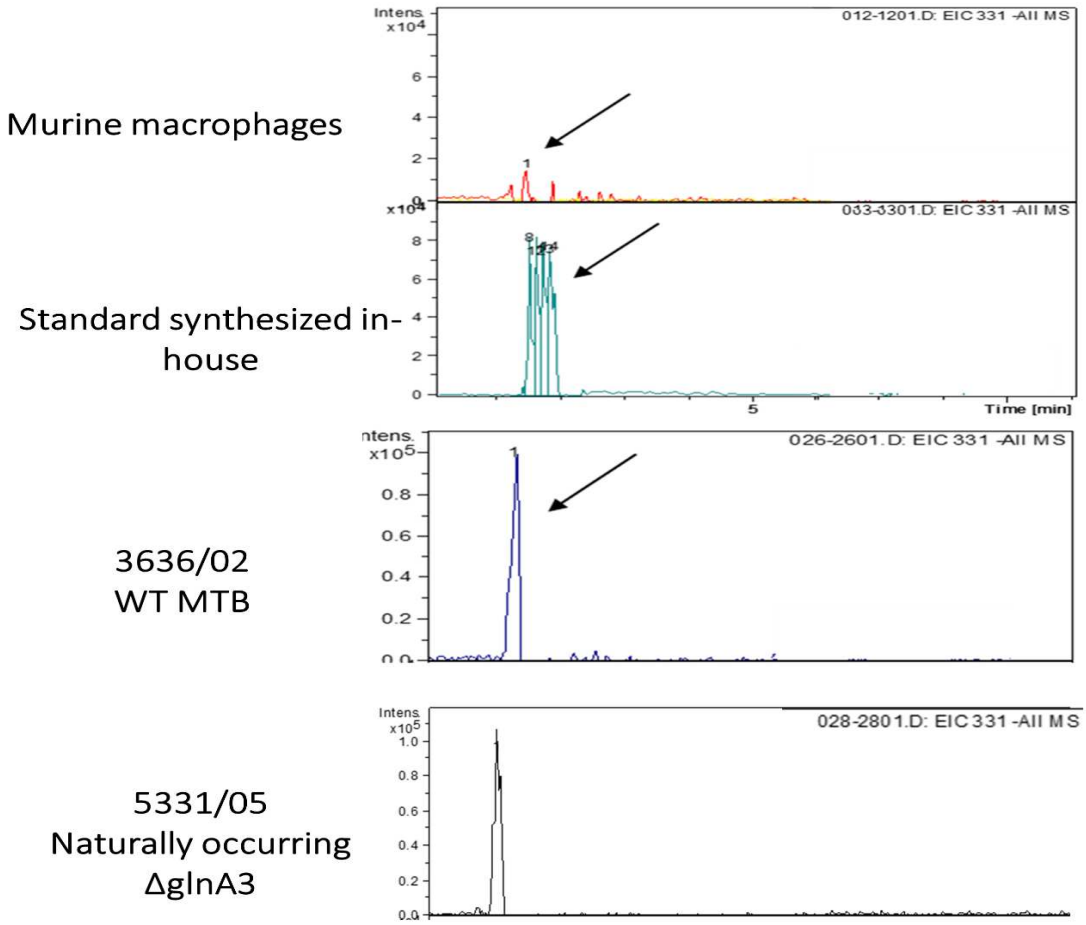

Suppl. Fig. 7. HPLC/ESI-MS detection of gamma-glutamylspermine in the MTB Beijing strain (WT variant) and in the naturally occurring *glnA3* Beijing mutant. Samples were analyzed in MS negative mode.

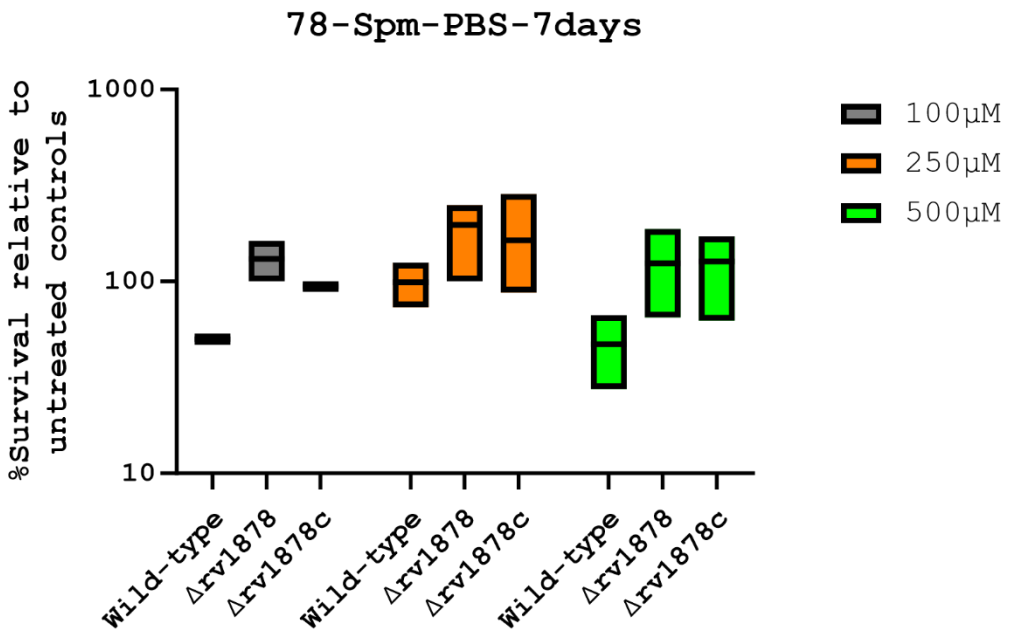

Suppl. Fig. 8. Spermine enhances the survival of the Δ*glnA3* mutant as a sole C/N source.Logarithmic phase cultures (in Sauton's media), were washed several times in PBS, diluted to approximately 10^5 CFUs/ml, and incubated in the presence (treated) or absence (untreated) of various concentrations of spermine over 7 days. Survival was determined by dividing the number of colonies obtained (after plating strains from various conditions) from the treated conditions to the untreated condition.

761

762

763

References

1. WHO. 2022. Global tuberculosis report; Geneva; Licence: CC BY-NC-SA 3.0 IGO.
2. Pai M, Behr MA, Dowdy D, Dheda K, Divangahi M, Boehme CC, Ginsberg A, Swaminathan S, Spigelman M, Getahun H. 2016. Tuberculosis. Nat Rev Dis Primers 2:16076.
3. Miller-Fleming L, Olin-Sandoval V, Campbell K, Ralser M. 2015. Remaining Mysteries of Molecular Biology: The Role of Polyamines in the Cell. J Mol Biol 427:3389-406.
4. Kusano T, Suzuki H. 2015. Polyamines: a universal molecular nexus for growth, survival, and specialized metabolism. Springer, Tokyo.
5. Davis RH, Ristow JL. 1991. Polyamine toxicity in Neurospora crassa: Protective role of the vacuole. Arch Biochem Biophys 285:306-311.
6. Pegg AE. 2013. Toxicity of Polyamines and Their Metabolic Products. Chem Res Toxicol 26:1782-1800.
7. Lasbury ME, Merali S, Durant PJ, Tschang D, Ray CA, Lee CH. 2007. Polyamine-mediated apoptosis of alveolar macrophages during Pneumocystis pneumonia. J Biol Chem 282:11009-20.
8. Tome EM, Fliser MS, Payne MC, Gerner WE. 1997. Excess putrescine accumulation inhibits the formation of modified eukaryotic initiation factor 5A (eIF-5A) and induces apoptosis. Biochem J 328:847-854.
9. Norris V, Reusch RN, Igarashi K, Root-Bernstein R. 2015. Molecular complementarity between simple, universal molecules and ions limited phenotype space in the precursors of cells. Biol Direct 10:1-20.
10. Schneider BL, Reitzer L. 2012. Pathway and enzyme redundancy in putrescine catabolism in Escherichia coli. J Bacteriol 194:4080-4088.
11. Kurihara S, Oda S, Tsuboi Y, Kim HG, Oshida M, Kumagai H, Suzuki H. 2008. gamma-Glutamylputrescine synthetase in the putrescine utilization pathway of Escherichia coli K-12. J Biol Chem 283:19981-90.
12. Yao X, He W, Lu CD. 2011. Functional characterization of seven gamma-Glutamylpolyamine synthetase genes and the bauRABCD locus for polyamine and beta-Alanine utilization in Pseudomonas aeruginosa PAO1. J Bacteriol 193:3923-30.
13. Foster A, Barnes N, Speight R, Keane MA. 2013. Genomic organisation, activity and distribution analysis of the microbial putrescine oxidase degradation pathway. Syst Appl Microbiol 36:457-466.
14. Forouhar F, Lee I-S, Vujcic J, Vujcic S, Shen J, Vorobiev SM, Xiao R, Acton TB, Montelione GT, Porter CW. 2005. Structural and functional evidence for Bacillus subtilis PaiA as a novel N1-spermidine/spermine acetyltransferase. J Biol Chem 280:40328-40336.
15. Campilongo R, Di Martino ML, Marcocci L, Pietrangeli P, Leuzzi A, Grossi M, Casalino M, Nicoletti M, Micheli G, Colonna B. 2014. Molecular and functional profiling of the polyamine content in enteroinvasive E. coli: looking into the gap between commensal E. coli and harmful Shigella. PloS One 9:e106589.
16. Krysenko S, Okoniewski N, Kulik A, Matthews A, Grimpo J, Wohlleben W, Bera A. 2017. Gamma-Glutamylpolyamine Synthetase GlnA3 Is Involved in the First Step of Polyamine Degradation Pathway in Streptomyces coelicolor M145. Front Microbiol 8:726.
17. Krysenko S, Okoniewski N, Nentwich M, Matthews A, Bäuerle M, Zinser A, Busche T, Kulik A, Gursch S, Kemeny A. 2022. A second gamma-Glutamylpolyamine synthetase,

GlnA2, is involved in polyamine catabolism in Streptomyces coelicolor. Int J Mol Sci 23:3752.

18. Krysenko S, Matthews A, Busche T, Bera A, Wohlleben W. 2021. Poly- and Monoamine Metabolism in Streptomyces coelicolor: The New Role of Glutamine Synthetase-Like Enzymes in the Survival under Environmental Stress. Microb Physiol 31:233-247.
19. Harth G, Clemens DL, Horwitz MA. 1994. Glutamine synthetase of Mycobacterium tuberculosis: extracellular release and characterization of its enzymatic activity. Proc Natl Acad Sci U S A 91:9342-9346.
20. Rexer H, Schäberle T, Wohlleben W, Engels A. 2006. Investigation of the functional properties and regulation of three glutamine synthetase-like genes in Streptomyces coelicolor A3 (2). Arch Microbiol 186:447-458.
21. Malm S, Tiffert Y, Micklinghoff J, Schultze S, Joost I, Weber I, Horst S, Ackermann B, Schmidt M, Wohlleben W, Ehlers S, Geffers R, Reuther J, Bange FC. 2009. The roles of the nitrate reductase NarGHJI, the nitrite reductase NirBD and the response regulator GlnR in nitrate assimilation of Mycobacterium tuberculosis. Microbiology (Reading) 155:1332-1339.
22. Tiffert Y, Supra P, Wurm R, Wohlleben W, Wagner R, Reuther J. 2008. The Streptomyces coelicolor GlnR regulon: identification of new GlnR targets and evidence for a central role of GlnR in nitrogen metabolism in actinomycetes. Mol Microbiol 67:861-80.
23. Krysenko S, Wohlleben W. 2022. Polyamine and ethanolamine metabolism in bacteria as an important component of nitrogen assimilation for survival and pathogenicity. Med Sci (Basel) 10:40.
24. Gawronski JD, Benson DR. 2004. Microtiter assay for glutamine synthetase biosynthetic activity using inorganic phosphate detection. Anal Biochem 327:114-8.
25. Waterhouse A, Bertoni M, Bienert S, Studer G, Tauriello G, Gumienny R, Heer FT, de Beer TAP, Rempfer C, Bordoli L. 2018. SWISS-MODEL: homology modelling of protein structures and complexes. Nucleic Acids Res 46:W296-W303.
26. Gill HS, Pfluegl GM, Eisenberg D. 2002. Multicopy crystallographic refinement of a relaxed glutamine synthetase from Mycobacterium tuberculosis highlights flexible loops in the enzymatic mechanism and its regulation. Biochemistry 41:9863-9872.
27. Krajewski WW, Jones TA, Mowbray SL. 2005. Structure of Mycobacterium tuberculosis glutamine synthetase in complex with a transition-state mimic provides functional insights. Proc Natl Acad Sci U S A 102:10499-10504.
28. Nilsson MT, Mowbray SL. 2012. Crystal structure of Mycobacterium tuberculosis glutamine synthethase in complex with imidazopyridine inhibitor ((4-(6-Bromo-3-(Butylamino)imidazo(1,2-A)Pyridin-2-YL)Phenoxy) Acetic acid) and L-Methionine-S-Sulfoximine phosphate. MedChemComm 3:620.
29. Nilsson MT, Mowbray SL. 2012. Crystal structure of Mycobacterium Tuberculosis Glutamine Synthetase in complex with tri-substituted imidazole inhibitor (4-(2-tert-butyl-4-(6-methoxynaphthalen-2-yl)-1H-imidazol-5-yl)pyridin-2-amine) and L- methionine-S-sulfoximine phosphate. J Med Chem 55.
30. Nilsson MT, Krajewski WW, Yellagunda S, Prabhumurthy S, Chamarahally GN, Siddamadappa C, Srinivasa BR, Yahiaoui S, Larhed M, Karlén A. 2009. Structural basis for the inhibition of Mycobacterium tuberculosis glutamine synthetase by novel ATP-competitive inhibitors. J Mol Biol 393:504-513.
31. Benkert P, Biasini M, Schwede T. 2011. Toward the estimation of the absolute quality of individual protein structure models. Bioinformatics 27:343-350.
32. Hooft RW, Sander C, Vriend G. 1997. Objectively judging the quality of a protein structure from a Ramachandran plot. Bioinformatics 13:425-430.

33. Chen VB, Arendall WB, Headd JJ, Keedy DA, Immormino RM, Kapral GJ, Murray LW, Richardson JS, Richardson DC. 2010. MolProbity: all-atom structure validation for macromolecular crystallography. Acta Crystallogr D Biol Crystallogr 66:12-21.
34. Ladner JE, Atanasova V, Dolezelova Z, Parsons JF. 2012. Structure and activity of PA5508, a hexameric glutamine synthetase homologue. Biochemistry 51:10121-10123.
35. Chanphai P, Thomas T, Tajmir-Riahi H. 2016. Conjugation of biogenic and synthetic polyamines with serum proteins: a comprehensive review. Int J Biol Macromol 92:515-522.
36. Parish T, Stoker NG. 2000. Use of a flexible cassette method to generate a double unmarked Mycobacterium tuberculosis tlyA plcABC mutant by gene replacement. Microbiology (Reading) 146:1969-1975.
37. Sao Emani C, Williams MJ, Van Helden PD, Taylor MJC, Carolis C, Wiid IJ, Baker B. 2018. Generation and characterization of thiol-deficient Mycobacterium tuberculosis mutants. Sci Data 5:180184.
38. Sassetti CM, Boyd DH, Rubin EJ. 2003. Genes required for mycobacterial growth defined by high density mutagenesis. Mol Microbiol 48:77-84.
39. Bosch B, DeJesus MA, Poulton NC, Zhang W, Engelhart CA, Zaveri A, Lavalette S, Ruecker N, Trujillo C, Wallach JB, Li S, Ehrt S, Chait BT, Schnappinger D, Rock JM. 2021. Genome-wide gene expression tuning reveals diverse vulnerabilities of M. tuberculosis. Cell 184:4579-4592 e24.
40. Adhikary A, Biswal S, Ghosh AS. 2022. The Putative Major Facilitator Superfamily (MFS) Protein Named Rv1877 in Mycobacterium tuberculosis Behaves as a Multidrug Efflux Pump. Curr Microbiol 79:324.
41. De Rossi E, Branzoni M, Cantoni R, Milano A, Riccardi G, Ciferri O. 1998. Mmr, a Mycobacterium tuberculosis gene conferring resistance to small cationic dyes and inhibitors. J Bacteriol 180:6068-6071.
42. Zelmer A, Carroll P, Andreu N, Hagens K, Mahlo J, Redinger N, Robertson BD, Wiles S, Ward TH, Parish T, Ripoll J, Bancroft GJ, Schaible UE. 2012. A new in vivo model to test anti-tuberculosis drugs using fluorescence imaging. J Antimicrob Chemother 67:1948-60.
43. Carroll P, Schreuder LJ, Muwanguzi-Karugaba J, Wiles S, Robertson BD, Ripoll J, Ward TH, Bancroft GJ, Schaible UE, Parish T. 2010. Sensitive detection of gene expression in mycobacteria under replicating and non-replicating conditions using optimized far-red reporters. PLoS One 5:e9823.
44. Shaner NC, Campbell RE, Steinbach PA, Giepmans BN, Palmer AE, Tsien RY. 2004. Improved monomeric red, orange and yellow fluorescent proteins derived from Discosoma sp. red fluorescent protein. Nat Biotechnol 22:1567-72.
45. Evans CGT, Herbert D, Tempest DW. 1970. Chapter XIII The Continuous Cultivation of Micro-organisms: 2. Construction of a Chemostat. Methods in Microbiology 2:277-327.
46. Gust B, Challis GL, Fowler K, Kieser T, Chater KF. 2003. PCR-targeted Streptomyces gene replacement identifies a protein domain needed for biosynthesis of the sesquiterpene soil odor geosmin. Proc Natl Acad Sci U S A 100:1541-1546.
47. Kieser T, Bibb MJ, Buttner MJ, Chater KF, Hopwood DA. 2000. Practical streptomyces genetics, vol 291. John Innes Foundation Norwich, Berlin.
48. Krysenko S, Matthews A, Okoniewski N, Kulik A, Girbas MG, Tsypik O, Meyners CS, Hausch F, Wohlleben W, Bera A. 2019. Initial metabolic step of a novel ethanolamine utilization pathway and its regulation in Streptomyces coelicolor M145. MBio 10:e00326-19.
49. Bullock WO, Fernandez JM, Short JM. 1987. XL1-blue: a high efficiency plasmid transforming recA Escherichia coli strain with beta-galactosidase selection. BioTechniques 5:376.

50. Simon R, Priefer U, Pühler A. 1983. A broad host range mobilization system for in vivo genetic engineering: transposon mutagenesis in gram negative bacteria. Bio/Technology 1:784-791.
51. Davanloo P, Rosenberg AH, Dunn JJ, Studier FW. 1984. Cloning and expression of the gene for bacteriophage T7 RNA polymerase. Proc Natl Acad Sci U S A 81:2035-2039.
52. Menges R, Muth G, Wohlleben W, Stegmann E. 2007. The ABC transporter Tba of Amycolatopsis balhimycina is required for efficient export of the glycopeptide antibiotic balhimycin. Appl Microbiol Biotechnol 77:125-134.
53. Pridmore RD. 1987. New and versatile cloning vectors with kanamycin-resistance marker. Gene 56:309-312.
54. Kubica GP, Kim TH, Dunbar FP. 1972. Designation of strain H37Rv as the neotype of Mycobacterium tuberculosis. Int J Syst Evol Microbiol 22:99-106.
55. Jumde RP, Guardigni M, Gierse RM, Alhayek A, Zhu D, Hamid Z, Johannsen S, Elgaher WA, Neusens PJ, Nehls C. 2021. Hit-optimization using target-directed dynamic combinatorial chemistry: development of inhibitors of the anti-infective target 1-deoxy-d-xylulose-5-phosphate synthase. Chem Sci 12:7775-7785.
56. Wallace RJ, Nash DR, Steele LC, Steingrube V. 1986. Susceptibility Testing of Slowly Growing Mycobacteria by a Microdilution MIC Method with 7H9 Broth. J Clin Microbiol 24:976-981.
57. Palomino JC, Martin A, Camacho M, Guerra H, Swings J, Portaels F. 2002. Resazurin microtiter assay plate: simple and inexpensive method for detection of drug resistance in Mycobacterium tuberculosis. Antimicrob Agents Chemother 46:2720-2.
58. Merker M, Kohl TA, Roetzer A, Truebe L, Richter E, Rusch-Gerdes S, Fattorini L, Oggioni MR, Cox H, Varaine F, Niemann S. 2013. Whole genome sequencing reveals complex evolution patterns of multidrug-resistant Mycobacterium tuberculosis Beijing strains in patients. PLoS One 8:e82551.
59. Andreu N, Zelmer A, Fletcher T, Elkington PT, Ward TH, Ripoll J, Parish T, Bancroft GJ, Schaible U, Robertson BD, Wiles S. 2010. Optimisation of bioluminescent reporters for use with mycobacteria. PLoS One 5:e10777.
60. Biasini M, Bienert S, Waterhouse A, Arnold K, Studer G, Schmidt T, Kiefer F, Cassarino TG, Bertoni M, Bordoli L. 2014. SWISS-MODEL: modelling protein tertiary and quaternary structure using evolutionary information. Nucleic Acids Res 42:W252-W258.
61. Altschul SF, Pop M. 2017. Sequence Alignment, 2nd ed. CRC Press/Taylor & Francis, Boca Raton (FL).
62. Remmert M, Biegert A, Hauser A, Söding J. 2012. HHblits: lightning-fast iterative protein sequence searching by HMM-HMM alignment. Nat Methods 9:173-175.
63. Bertoni M, Kiefer F, Biasini M, Bordoli L, Schwede T. 2017. Modeling protein quaternary structure of homo-and hetero-oligomers beyond binary interactions by homology. Sci Rep 7:1-15.
64. Biasini M, Schmidt T, Bienert S, Mariani V, Studer G, Haas J, Johner N, Schenk AD, Philippsen A, Schwede T. 2013. OpenStructure: an integrated software framework for computational structural biology. Acta Crystallogr D Biol Crystallogr 69:701-709.
65. Guex N, Peitsch MC. 1997. SWISS-MODEL and the Swiss-Pdb Viewer: an environment for comparative protein modeling. Electrophoresis 18:2714-2723.
66. Zheng L, Baumann U, Reymond J-L. 2004. An efficient one-step site-directed and site-saturation mutagenesis protocol. Nucleic Acids Res 32:e115-e115.
67. Li H, Durbin R. 2009. Fast and accurate short read alignment with Burrows-Wheeler transform. Bioinformatics 25:1754-60.
68. Liao Y, Smyth GK, Shi W. 2014. featureCounts: an efficient general purpose program for assigning sequence reads to genomic features. Bioinformatics 30:923-30.
69. Robinson MD, Oshlack A. 2010. A scaling normalization method for differential expression analysis of RNA-seq data. Genome Biol 11:R25.

70. Robinson MD, McCarthy DJ, Smyth GK. 2010. edgeR: a Bioconductor package for differential expression analysis of digital gene expression data. Bioinformatics 26:139-40.
71. Latour YL, Gobert AP, Wilson KT. 2020. The role of polyamines in the regulation of macrophage polarization and function. Amino Acids 52:151-160.
72. Hirsch JG, Dubos RJ. 1952. The effect of spermine on tubercle bacilli. J Exp Med 95:191-208.
73. Joshi GS, Spontak JS, Klapper DG, Richardson AR. 2011. Arginine catabolic mobile element encoded speG abrogates the unique hypersensitivity of Staphylococcus aureus to exogenous polyamines. Mol Microbiol 82:9-20.
74. Yao X, Lu CD. 2014. Characterization of Staphylococcus aureus responses to spermine stress. Curr Microbiol 69:394-403.
75. Tullius MV, Harth G, Horwitz MA. 2003. Glutamine synthetase GlnA1 is essential for growth of Mycobacterium tuberculosis in human THP-1 macrophages and guinea pigs. Infect Immun 71:3927-36.
76. Kruh NA, Troudt J, Izzo A, Prenni J, Dobos KM. 2010. Portrait of a pathogen: the Mycobacterium tuberculosis proteome in vivo. PLoS One 5:e13938.
77. Cole S, Brosch R, Parkhill J. et al. 1998. Deciphering the biology of Mycobacterium tuberculosis from the complete genome sequence. Nature 393:537-540.
78. De Rossi E, Arrigo P, Bellinzoni M, Silva PEA, Martin C, Ainsa JA, Guglierame P, Riccardi G. 2002. The multidrug transporters belonging to major facilitator superfamily (MFS) in Mycobacterium tuberculosis. Mol Med 8:714-724.
79. Grinius LD, G., Goldberg EB, Liao CH, Projan SJ. 1992. A staphylococcal multidrug resistance gene product is a member of a new protein family. Plasmid 27:119-129.
80. Dutta NK, Mehra S, Kaushal D. 2010. A Mycobacterium tuberculosis sigma factor network responds to cell-envelope damage by the promising anti-mycobacterial thioridazine. PLoS One 5:e10069.

81. Balganesh M, Dinesh N, Sharma S, Kuruppath S, Nair AV, Sharma U. 2012. Efflux pumps of *Mycobacterium tuberculosis* play a significant role in antituberculosis activity of potential drug candidates. Antimicrob Agents Chemother. 56(5): 2643-2651.